

8-1-2019

## Newly defined ATP-binding cassette subfamily B member 5 positive dermal mesenchymal stem cells promote healing of chronic iron-overload wounds via secretion of interleukin-1 receptor antagonist

Seppe Vander Beken

Juliane C. de Vries

Barbara Meier-Schiesser

Patrick Meyer

Dongsheng Jiang

*See next page for additional authors*

Follow this and additional works at: <https://ro.ecu.edu.au/ecuworkspost2013>



Part of the [Medicine and Health Sciences Commons](#)

---

10.1002/stem.3022 Vander Beken, S., de Vries, J. C., Meier-Schiesser, B., Meyer, P., Jiang, D., Sindrilaru, A., ... Scharffetter-Kochanek, K. (2019). Newly defined ATP-binding cassette subfamily B member 5 positive dermal mesenchymal stem cells promote healing of chronic iron-overload wounds via secretion of interleukin-1 receptor antagonist. *Stem Cells*, 37(8), 1057-1074. Available [here](#)

This Journal Article is posted at Research Online.

<https://ro.ecu.edu.au/ecuworkspost2013/6560>

---

## Authors

Seppe Vander Beken, Juliane C. de Vries, Barbara Meier-Schiesser, Patrick Meyer, Dongsheng Jiang, Anca Sindrilaru, Filipa F. Ferreira, Adelheid Hainzl, Susanne Schatz, Jana Muschhammer, Natalie J. Scheurmann, Panagiotis Kampilafkos, Andreas M. Seitz, Lutz Dürselen, Anita Ignatius, Mark A. Kluth, Christoph Ganss, Meinhard Wlaschek, Karmveer Singh, Pallab Maity, Natasha Y. Frank, Markus H. Frank, and Karin Scharffetter-Kochanek



# BioStudio -T


## Cell Observation Device

---

Nikon's BioStudio-T was designed specifically for research applications in the field of regenerative medicine and stem cell biology and for use in cell manufacturing facilities. A compact live-cell imaging microscope, the BioStudio-T fits inside most incubators and is compatible with a variety of sterilization methods including vaporized H<sub>2</sub>O<sub>2</sub>. The fixed-stage, scanning lens system also provides a superior solution for long-term time lapse imaging and large image acquisition.

For more information on the BioStudio-T,  
visit [www.microscope.healthcare.nikon.com/biostudio-t](http://www.microscope.healthcare.nikon.com/biostudio-t)

# Newly Defined ATP-Binding Cassette Subfamily B Member 5 Positive Dermal Mesenchymal Stem Cells Promote Healing of Chronic Iron-Overload Wounds via Secretion of Interleukin-1 Receptor Antagonist

SEPPE VANDER BEKEN,<sup>a</sup> JULIANE C. DE VRIES,<sup>a</sup> BARBARA MEIER-SCHIESSER,<sup>a</sup> PATRICK MEYER,<sup>a</sup> DONGSHENG JIANG,<sup>a</sup> ANCA SINDRILARU,<sup>a</sup> FILIPA F. FERREIRA,<sup>a</sup> ADELHEID HAINZL,<sup>a</sup> SUSANNE SCHATZ,<sup>a</sup> JANA MUSCHHAMMER,<sup>a</sup> NATALIE J. SCHEURMANN,<sup>a</sup> PANAGIOTIS KAMPILAFKOS,<sup>a</sup> ANDREAS M. SEITZ,<sup>b</sup> LUTZ DÜRSELEN,<sup>b</sup> ANITA IGNATIUS,<sup>b</sup> MARK A. KLUTH,<sup>c,d</sup> CHRISTOPH GANSS,<sup>c,d</sup> MEINHARD WLASCHEK,<sup>a</sup> KARMVEER SINGH ,<sup>a</sup> PALLAB MAITY,<sup>a</sup> NATASHA Y. FRANK,<sup>e,f,g</sup> MARKUS H. FRANK,<sup>e,h,i,j</sup> KARIN SCHARFFETTER-KOCHANÉK<sup>a</sup>

**Key Words.** Clinical translation • Cell surface markers • Mesenchymal stem cells • Tissue regeneration • Tissue-specific stem cells • Xenotransplantation

<sup>a</sup>Department of Dermatology and Allergic Diseases, Ulm University, Ulm, Germany;

<sup>b</sup>Institute of Orthopaedic Research and Biomechanics, Ulm University, Ulm, Germany; <sup>c</sup>TICEBA GmbH, Heidelberg, Germany; <sup>d</sup>RHEACELL GmbH & Co. KG, Heidelberg, Germany;

<sup>e</sup>Transplantation Research Center, Boston Children's Hospital and Brigham and Women's Hospital, Boston, Massachusetts, USA;

<sup>f</sup>Department of Medicine, Boston VA Healthcare System, Boston, Massachusetts, USA;

<sup>g</sup>Division of Genetics, Brigham and Women's Hospital, Harvard Medical School, Boston, Massachusetts, USA; <sup>h</sup>Harvard Skin Disease Research Center, Department of Dermatology, Brigham and Women's Hospital, Harvard Medical School, Boston, Massachusetts, USA; <sup>i</sup>Harvard Stem Cell Institute, Harvard University, Cambridge, Massachusetts, USA; <sup>j</sup>School of Medical and Health Sciences, Edith Cowan University, Perth, Western Australia, Australia

Correspondence: Karin Scharffetter-Kochanek, M.D., Ph.D., Department of Dermatology and Allergic Diseases, Ulm University, Ulm, Germany. Telephone: 0049073150057501; e-mail: karin.scharffetter-kochanek@uniklinik-ulm.de

Received October 17, 2018; accepted for publication February 22, 2019; first published online April 19, 2019.

<http://dx.doi.org/10.1002/stem.3022>

This is an open access article under the terms of the Creative Commons Attribution-NonCommercial License, which permits use, distribution and reproduction in any medium, provided the original work is properly cited and is not used for commercial purposes.

## ABSTRACT

In this study, we report the beneficial effects of a newly identified dermal cell subpopulation expressing the ATP-binding cassette subfamily B member 5 (ABCB5) for the therapy of nonhealing wounds. Local administration of dermal ABCB5<sup>+</sup>-derived mesenchymal stem cells (MSCs) attenuated macrophage-dominated inflammation and thereby accelerated healing of full-thickness excisional wounds in the iron-overload mouse model mimicking the nonhealing state of human venous leg ulcers. The observed beneficial effects were due to interleukin-1 receptor antagonist (IL-1RA) secreted by ABCB5<sup>+</sup>-derived MSCs, which dampened inflammation and shifted the prevalence of unrestrained proinflammatory M1 macrophages toward repair promoting anti-inflammatory M2 macrophages at the wound site. The beneficial anti-inflammatory effect of IL-1RA released from ABCB5<sup>+</sup>-derived MSCs on human wound macrophages was conserved in humanized NOD-*scid* IL2r<sup>γ</sup><sup>null</sup> mice. In conclusion, human dermal ABCB5<sup>+</sup> cells represent a novel, easily accessible, and marker-enriched source of MSCs, which holds substantial promise to successfully treat chronic non-healing wounds in humans. *STEM CELLS* 2019;37:1057–1074

## SIGNIFICANCE STATEMENT

The ATP-binding cassette protein ATP-binding cassette subfamily B member 5 (ABCB5), a single molecular marker, can be used to isolate dermal cell subpopulation of the skin with multipotent mesenchymal stromal cell (MSC) characteristics from its endogenous niche. The ABCB5<sup>+</sup> MSCs maintain most of their stemness and mesenchymal marker during large in vitro expansion cultures as well as the capacity for clonal self-renewal and, importantly, promote healing of non-healing iron-overload wounds in a murine model, which may be exploited as a potential regenerative therapy for chronic venous leg ulcers in human patients.

## INTRODUCTION

Although poorly defined, self-renewing adult pluripotent mesenchymal stem cells (MSCs) reside within nearly all adult connective tissues, including the dermis [1, 2]. Their most important function is to maintain their niche environment, a critical requirement to protect their own stemness and long-term self-renewal capacity essential for tissue homeostasis, repair, and organ maintenance [3].

Due to their capacity to engraft and release wound healing-promoting factors, profound interest has developed in advanced MSC-based therapies for patients suffering from acute and chronic wounds. To date, 1% to 2% of the population in developed countries suffer from a non-healing wound, and the incidence of chronic wounds is estimated to increase due to the world-wide increase in elderly, obese, and diabetic patients [4]. One major hurdle still hampering the successful implementation of large-scale

MSC-based therapies in clinical practice is the lack of a cell surface marker that reliably allows to enrich and expand MSCs for reproducible paracrine efficacy and potency.

Recently, we showed that ATP-binding cassette subfamily B member 5 (ABCB5) identifies a novel dermal immunomodulatory subpopulation, which in addition expresses MSC markers and exerts suppressive effects on effector T cells, whereas enhancing regulatory T cells in vitro and in vivo [5]. ABCB5 belongs to the multiple drug resistant cell membrane-anchored proteins that are also expressed on limbal stem cells of the eye where its absence results in blindness [6]. By means of specific antibodies, we here show that the ABCB5<sup>+</sup> dermal MSC population can reliably be isolated according to GMP standards and thus holds substantial promise to define a more homogeneous MSC population for large-scale expansion with improved efficacy and potency, urgently required for advanced treatment of chronic wounds.

Although different in etiology, chronic wounds share the common feature of persistent high numbers of overactivated proinflammatory M1 macrophages [7, 8] with enhanced release of tumor necrosis factor alpha (TNF $\alpha$ ) and other proinflammatory cytokines. These proinflammatory cytokines along with proteases and reactive oxygen species lead to tissue breakdown and the installment of a senescence program in resident wound site fibroblasts, thus perpetuating a nonhealing state of these wounds. We previously identified iron accumulation in macrophages residing in chronic venous leg ulcers as a consequence of persistent extravasation of red blood cells at the wound site due to increased blood pressure and venous valve insufficiency. Iron overloaded macrophages in these wounds fail to switch from their proinflammatory M1 state to anti-inflammatory M2 macrophages required for tissue remodeling and restoration [7]. M2 macrophages show a lower inflammatory cytokine release as opposed to their M1 counterparts and produce growth factors and metabolites that stimulate tissue repair and wound healing [9]. Conversely, effector molecules like TNF $\alpha$  and interleukin-1  $\beta$  (IL-1 $\beta$ ), among others released by M1 macrophages, maintain a vicious cycle of autocrine recruitment and constant activation of M1 macrophages, thus virtually locking wounds in a nonhealing state of persistent inflammation [7, 8].

We here specifically addressed the involvement of paracrine mechanisms used by ABCB5<sup>+</sup>-derived MSCs to counteract persisting inflammation and to switch the prevailing M1 macrophages toward tissue repair promoting M2 macrophages, a prerequisite for healing of chronic wounds.

To exclude any engraftment or cell fusion effects, we purposely used a xenotransplant model with local injection of human ABCB5<sup>+</sup>-derived MSCs into chronic wounds of the iron-overload murine model closely mirroring the major pathogenic aspect of unrestrained M1 macrophage activation in human chronic wounds [7]. We have used clinical grade approved ABCB5<sup>+</sup> MSC preparations with documented clonal trilineage differentiation capacity, enhanced clonal growth, and TNF $\alpha$  suppressing activity in vitro as valuable predictors for successful treatment of chronic wounds in vivo. We found that ABCB5<sup>+</sup>-derived MSCs injected into iron-overload wounds enhanced release of the paracrine IL-1 receptor antagonist (IL-1RA) and, indeed, switched the prevailing M1 proinflammatory macrophage phenotype excessively increased in chronic iron-overload murine wounds to an anti-inflammatory M2 macrophage promoting overall wound healing. The causal role of the paracrine release of IL-1RA from injected

ABCB5<sup>+</sup>-derived MSCs was supported by our findings that injection of human recombinant IL-1RA accelerated wound healing, whereas injection of IL-1RA silenced ABCB5<sup>+</sup>-derived MSCs did not. Notably, these data are recapitulated in humanized NOD-*scid* IL2 $\gamma$ <sup>null</sup> (NSG) mice, with a shift from human proinflammatory M1 to anti-inflammatory M2 macrophages further paving the way for the successful translation of marker-enriched ABCB5<sup>+</sup> MSCs therapies into clinical practice for the long-term benefit of our patients.

## MATERIALS AND METHODS

### Study Design

The purpose of this study was to determine whether human dermal ABCB5<sup>+</sup> cells are MSCs and have beneficial effects on chronic wound healing in cellular therapeutic applications. In vitro, ABCB5<sup>+</sup> MSCs and donor-matched ABCB5<sup>-</sup> human dermal fibroblasts (HDFs) from at least six different donors (Supporting Information Table S1: B02-B07) were tested for MSC-characteristic trilineage differentiation, surface marker expression, clonogenic growth, self-renewal, and anti-inflammatory effects on activated macrophages by quantitative measures. In vivo, improvement on wound healing by anti-inflammatory mechanisms was assessed in the mouse iron-overload full-thickness excisional wound model for chronic venous ulcers, characterized by delayed wound closure, prolonged inflammation, and M1-activated macrophage abundance [7]. For these animal studies, sample sizes were estimated based on differences in wound closure from our previous study identifying delayed wound healing in genetically modified mice [10] in order to reach a significance level of 5% and a statistical power of 80% by the Welch's test, with the inclusion of one additional animal (four wounds) to protect against deviations from the Gaussian distribution. Key animal experiments with ABCB5<sup>+</sup>-derived MSCs and donor-matched ABCB5<sup>-</sup> HDF injection were performed 3 times with cells from three different donors (Supporting Information Table S1: B01, B13, B14). Repetition experiments for sample collection were performed with human dermal cells either from the donor with internal number B01 (Supporting Information Table S1) for which cell preparation purities (Fig. 2A) and wound closure data (Fig. 3F, 3G) are shown here or with a phenotypically and functionally verified pooled sample of cells from six different donors (Supporting Information Fig. S4 and Table S1). This pooled dermal ABCB5<sup>+</sup>-derived MSC preparation was also used for IL-1RA knockdown and humanized NSG mouse wound closure experiments. The equal amount of cells derived from independent biological samples were analyzed in each quantitative assay. Microscopic images are representative for six wound samples per treatment group. Biological samples for analysis of xenografted ABCB5<sup>+</sup>-derived MSC persistence by human-specific beta actin quantitative polymerase chain reaction (qPCR) on wound sections and enzyme-linked immunosorbent assay (ELISA) quantification of wound cytokine titers are each pooled from two independent wounds and for hIL-1RA Western blot and wound macrophage flow cytometry from four independent wounds.

### Human Skin Samples

Skin biopsies used for the isolation of ABCB5<sup>+</sup> and ABCB5<sup>-</sup> cell fractions in this study measured 1 cm<sup>2</sup> and were either taken from

young healthy volunteers at the University Clinic of Dermatology and Allergic Diseases in Ulm or the University Clinic of Gynecology (skin from healthy females undergoing reduction mammoplasty; donors B02–B07) after approval by the ethical committee at Ulm University or directly derived from clients of Ticeba GmbH (Heidelberg, Germany; donors B01 and B08–B14) according to the Declaration of Helsinki principles after informed written consent was obtained. Localization was chosen to avoid isolation of cells from sun-exposed areas of the skin. The variation in localization (gluteal region, inner upper arm, or behind left ear) depended on surgical standards and donor preference. All biopsies were histologically assessed for any pathology. Only biopsies without pathology were used for immunostaining or for isolation of ABCB5<sup>+</sup> and ABCB5<sup>-</sup> cell fractions. None of the biopsies taken failed to yield ABCB5<sup>+</sup> cells. Anonymized donor data can be found in Supporting Information Table S1. Expansion of plastic-adherent dermal cells and ABCB5-based separation modified from Frank et al. [11] was performed as indicated (please see Supporting Information Materials and Methods for details). Cell viability was assessed before in vitro experiments, and no difference was found between both in the ABCB5<sup>+</sup> and ABCB5<sup>-</sup> population (>90%). Also, when harvesting ABCB5<sup>+</sup> MSCs and the ABCB5<sup>-</sup> cell fraction by Accutase for the injection into wounds, viability is routinely checked by trypan blue exclusion and is consistently very high (>90%) both in the ABCB5<sup>+</sup> and ABCB5<sup>-</sup> population.

Before application in in vivo wound-healing experiments, ABCB5<sup>+</sup> cell preparations were tested for their M1 macrophage suppressing function in a coculture with interferon- $\gamma$  (IFN- $\gamma$ )/Lipopolysaccharide (LPS)-activated murine bone marrow-derived macrophages, and the release of TNF $\alpha$  was assessed by a mouse-specific TNF $\alpha$  ELISA (R&D Systems, Germany; Figs. 3B, 6D; Supporting Information Fig. S4).

### Differentiation and Clonogenic Growth Assays

In vitro adipogenic, osteogenic, and chondrogenic differentiation capacity was examined using commercial differentiation media (Lonza, Germany) and TGF- $\beta$ 3 (CellSystems, Germany) and procedures according to manufacturer's descriptions. For adipogenic differentiation, lipid droplet accumulation was verified by staining with Oil Red O (Sigma-Aldrich, Germany) and quantified by dye extraction as described previously [12]. Mineralization of the extracellular matrix of osteoblasts was verified by Alizarin Red S staining (Sigma-Aldrich) and quantified by subsequent dye extraction as described [13]. To visualize chondrogenic differentiation, three-dimensional-micromass cultures were immunostained for Aggrecan (R&D Systems, AF1220) according to standard procedures (see section Histology and Immunofluorescence Staining). For quantification of chondrogenesis, cartilage-specific sulfated proteoglycans and glycosaminoglycans formed in the micromasses were measured using the Blyscan Glycosaminoglycan Assay kit (Biocolor, United Kingdom) according to the manufacturer's instructions. For assessment of clonogenic growth, ABCB5<sup>+</sup> dermal MSCs and donor-matched ABCB5<sup>-</sup> HDFs were seeded at a density of 200 cells per 100 mm culture dish. After 14 days, colonies were stained with 0.5% crystal violet (Sigma-Aldrich) and colonies  $\geq$ 25 cells were counted on three to five parallel dishes per sample. For clonal expansion assays, ABCB5<sup>+</sup>-derived MSCs were seeded at 100 cells per 100 mm culture dish. After 14 days, 12 colonies separated from neighboring colonies by at least one microscopic field

were picked and expanded. Well-growing clonal cultures were elected for secondary trilineage differentiation and clonogenic growth assays.

### Human and Mouse Macrophage Cocultures

Mouse bone marrow-derived macrophages were isolated from femurs and matured for 6 days with macrophage colony-stimulating factor (M-CSF) containing L929 cell supernatant supplementation as described [10]. Human macrophages were matured under presence of 20 ng/ml recombinant human M-CSF (Miltenyi Biotec, Germany) for 8 days from peripheral blood mononuclear cell (PBMC)-derived monocytes sorted for CD14 expression by positive magnetic bead selection (Miltenyi Biotec) with purity >95%. Fresh buffy coats for PBMC isolation by gradient centrifugation were obtained from the German Red Cross. For coculture experiments, ABCB5<sup>+</sup>-derived MSCs or donor-matched ABCB5<sup>-</sup> HDFs were plated to adhere at  $2 \times 10^4$  cells per well in 24-well plates in 0.5 ml Dulbecco's modified Eagle's medium with 10% high-quality fetal bovine serum, 100 U/ml penicillin/streptomycin and 2 mM L-glutamine. After 24 hours, macrophages were seeded on top at  $1 \times 10^5$  cells per well in 0.5 ml, resulting in a 1:5 cell ratio unless indicated differently. Cocultures were incubated with 50 U/ml recombinant mouse or human IFN- $\gamma$  (R&D Systems) for 24 hours and then stimulated with 20 ng/ml LPS (Sigma-Aldrich) and 50 U/ml IFN- $\gamma$  for another 24 hours period before supernatants were harvested and analyzed by ELISA (R&D Systems).

### Mice and Wound Healing Models

Both female C57BL/6N (Charles River, Germany, strain 027) and female or male NOD.Cg-Prkdc<sup>scid</sup> Il2rg<sup>tm1Wjl</sup>/SzJ (Jax strain 005557) mice were 10–12 weeks old at the start of experiments and held under specific pathogen-free conditions in individually vented cages at the animal facility of the Ulm University. Experiments were performed in compliance with the German law for welfare of laboratory animals and approved by the Baden-Württemberg governmental review board.

The C57BL/6 mouse model relevant for chronic venous ulcers (CVU) physiopathology was performed as described previously [7]. For cellular treatment with human dermal ABCB5<sup>+</sup>-derived MSCs or corresponding ABCB5<sup>-</sup> HDFs,  $1 \times 10^6$  cells suspended in phosphate-buffered saline (PBS) per mouse were injected into the dermis at three 50  $\mu$ l injection points around each wound edge.

For the assessment of wound closure, NSG mice were humanized with  $2 \times 10^7$  human PBMC in 200  $\mu$ l PBS by tail-vein injection as previously described [14] 8 days before wounding. At day 1 postwounding, mice were randomly assigned to treatment groups receiving intradermal injection of a six-donor pool ABCB5<sup>+</sup> MSC preparation (Supporting Information Table S1: B01 + B08 + B09 + B10 + B11 + B12), donor-matched ABCB5<sup>-</sup> HDFs, or PBS alone. For the assessment of macrophage phenotype shift, NSG mice were humanized 1 day before wounding. At day 1 postwounding, random groups were treated with either ABCB5<sup>+</sup> MSCs from donor B01 or PBS as described above. At day 5 after wounding, two independent wound halves of each mouse were processed for immunofluorescence staining, the others were pooled for flow cytometry.

### siRNA-Mediated Knockdown of IL-1RA Expression in ABCB5<sup>+</sup>-Derived MSCs

ABCB5<sup>+</sup>-derived MSCs were transiently transfected with 20 nM of either a combination of four siRNAs specific for human IL-1RA or with scrambled control-A siRNA with accompanying transfection medium at the minimum recommended concentration (all products from Santa Cruz Biotechnologies, Germany) according to manufacturer's instructions. Successful knockdown was tested at the protein level upon in vitro inflammatory stimulation with IFN- $\gamma$ /LPS-activated mouse bone marrow-derived macrophages and culture supernatant medium ELISA for human IL-1RA (R&D Systems) before use in in vivo experiments and was typically at ~80% as shown in Figure 5D.

### Histology and Immunofluorescence Staining

Human skin tissue samples were embedded in the O.C.T. compound (TissueTek, Germany), frozen at  $-80^{\circ}\text{C}$  processed to 5  $\mu\text{m}$  sections and fixed in acetone. Mouse wounds were fixed overnight with 4% paraformaldehyde (PFA), cut through the middle, paraffin embedded, and only the first series of 5  $\mu\text{m}$  sections were used to avoid the wound edges. Adherent cells were cultured on glass coverslips, fixed with 4% PFA and permeabilized with 0.5% TritonX-100 in PBS. Sections or slides were incubated with primary antibodies listed in Supporting Information (Table S3) that were diluted as per manufacturers recommendations in antibody diluent (DAKO, Germany) at  $4^{\circ}\text{C}$  overnight. Mouse anti-ABCB5 was used at a concentration of 14  $\mu\text{g}/\text{ml}$  and incubation of 40 minutes at  $37^{\circ}\text{C}$  for staining of cryosections and 4  $\mu\text{g}/\text{ml}$  at  $4^{\circ}\text{C}$  overnight for staining of adherent cells. After washing with PBS, sections or slides were incubated with either AlexaFluor488- or AlexaFluor555-conjugated corresponding secondary antibodies (all from Invitrogen, Germany). Nuclei were counterstained with DAPI before mounting in fluorescent mounting medium (DAKO). The background staining was controlled by appropriate isotype-matched control antibodies. The specificity of the anti-ABCB5 staining was assessed by a peptide competition assay, pre-incubating the antibody with a 200-fold molar excess of peptide of the epitope amino acid sequence [11] (RFGAYLIQAGRMTPEG, GeneCust) before immunofluorescence staining, showing a loss of the fluorescent signal.

Masson trichrome (Sigma-Aldrich) and picosirius red (Polysciences) stainings were performed as per manufacturer's instructions on paraffin sections, and picosirius red stained slides were analyzed with circularly polarized light. Images were captured with an AxioImager.M1 microscope, AxioCam MRc camera, and AxioVision software (Carl Zeiss, Germany).

### Human-Specific Beta Actin Sequence-Specific qPCR

Quantification of injected human ABCB5<sup>+</sup>-derived MSCs and ABCB5<sup>-</sup> HDFs within the mouse wound sections was performed by human-specific beta actin sequence PCR. Briefly, we have isolated the genomic DNA from PFA-fixed paraffin-embedded wound sections employing QIAamp DNA FFPE tissue kit (56,404, Qiagen) followed by PCR with human-specific beta actin primers (forward primer: CACCACCGCCGAGACCGC and reverse primer: GCTGGCCGGGCTTACCTG). Then densitometry analysis was performed to quantify the density of PCR product separated on the gel images and normalized with mouse-specific beta actin sequence PCR product. The PCR of mouse beta actin was

performed with mouse-specific beta actin primers (forward primer: CCTTCTTCTTGGGTAAGTTGTAGC and reverse primer: CCATACC TAAGAGAAGAGTGACAGAAATC).

### ELISAs and Western Blot

Frozen minced wound tissue samples were dissolved in RIPA buffer (Sigma) supplemented with protease-inhibitor cocktail (Roche) and the phosphatase inhibitors  $\text{Na}_3\text{VO}_4$  (2 mM) and NaF (10 mM) in Lysing D columns (MP Biomedicals, Germany) subjected to three rounds of 20 seconds cooled vibrational force. Protein yield was measured by Bradford assay and spectrophotometric analysis against a bovine serum albumin (BSA)-standard dilution. All ELISA assays were performed with DuoSet kits (R&D Systems) following manufacturer's instructions. Western blot analysis for IL-1RA was performed as earlier published [15]. A rabbit anti-IL-1RA IgG<sub>1</sub> antibody (Abcam, Germany #ab124962) which detects human and murine IL-1RA at a dilution of 1:1000 and a secondary HRP-coupled anti-rabbit IgG (H + L) antibody (Dianova, Germany) at a dilution of 1:10,000 were used. Equal loading was verified by actin. Chemiluminescence was detected after addition of LumiGLO chemiluminescent substrate (Cell Signaling, Germany) with a Vilber Fusion Fx7 (Vilber Lourmat, Germany).

### Flow Cytometry

Flow cytometry for ABCB5 was performed using anti-ABCB5 mouse IgG<sub>1</sub> (clone 3C2-1D12; [11]) and secondary AlexaFluor647-conjugated donkey anti-Mouse IgG (H + L) (Fisher Scientific, Germany). Multicolor labeling of cells for the MSC-marker panel CD90, CD73, and CD105 as well as for CD34, CD14, CD20, and CD45 was performed with the human MSC phenotyping kit (Miltenyi Biotec) following the manufacturer's instructions. Anti-human SSEA-4-PE, CD271-FITC, CD133, CD318, and Melan-A antibodies (Supporting Information Table S3) were incubated with the cells for 45 minutes at  $4^{\circ}\text{C}$  at concentrations recommended by the manufacturer. For the detection of CD133, CD318, and Melan-A, cells washed with fluorescence-activated cell sorting (FACS)-buffer (1% BSA in PBS) were subsequently incubated with fluorochrome-conjugated secondary antibodies for 45 minutes at  $4^{\circ}\text{C}$ . Dead cells were excluded by costaining with SYTOX Blue (Invitrogen). Isotype-matched control antibodies were used for setting of gates.

For wound macrophage isolation, mouse wounds were digested as previously described [16, 17]. Briefly, minced tissues were incubated with 1.5 mg/ml collagenase I and 1.5 mg/ml hyaluronidase I (Sigma-Aldrich) in HEPES-buffered saline for 1 hour at  $37^{\circ}\text{C}$ . Single cell preparations were filtered and incubated for 15 minutes with FcR blocking (MACS) before staining with antibodies listed in Supporting Information Table S3. Additional intracellular stainings were performed after fixation and permeabilization using a commercial kit (BD, Germany) according to the manufacturer's protocol. Blank and single-stained samples were used for photomultiplier (PMT) and compensation settings. For wound macrophages, singlet F4/80<sup>+</sup> mouse macrophages in C57BL/6N samples and singlet CD68<sup>+</sup> human macrophages in humanized NSG mouse samples were gated (Supporting Information Fig. S11) for subsequent M1 and M2 marker expression analysis based on relative fluorescence units (= geometric fluorescence intensity relative to isotype control sample) or % positive events within the macrophage population. Hereto, positivity thresholds were set against the relevant fluorescence-conjugated isotype

controls and macrophage gating marker stained control samples. Flow cytometry was performed on FACSCanto II, FACSARIA Fusion, or Accuri flow cytometers (BD Biosciences, Germany), and the data thereafter analyzed using FlowJo analysis software (TreeStar Inc., USA).

### Comprehensive Transcriptome Profiling and Quantitative PCR

To prepare the total RNAseq library, 500 ng of total RNA was used as input. First, 500 ng of total RNA was used to deplete the rRNA using a commercially available kit (Low Input Ribominus Eukaryotic System v2, Thermo, Germany) as described in the manual with slight modifications. In brief, after the rRNA was depleted using RiboMinus Eukaryote Probe Mix, the supernatant containing rRNA-depleted RNA was collected and incubated with 3x Agencourt RNAClean XP beads for 20 minutes on ice, followed by removal of supernatant and washing of RNAClean XP beads 2 times with 80% ethanol, and finally the rRNA depleted RNA was eluted from the beads in 10  $\mu$ l of nuclease-free water. This rRNA depleted RNA was used to prepare RNAseq library for Illumina platform using NEBNext Ultra II Directional RNA library prep kit (NEB, Germany) with some modifications. The quality control of the RNAseq libraries was performed by Agilent Bioanalyzer, and concentration of the libraries were measured in qubit using dsDNA HS assay kit (Thermo). The libraries were sequenced in Illumina NextSeq 500 system for 75 cycles (1  $\times$  75 single end reads) of sequencing and two index reads of eight cycles each using NextSeq 500/550 v2 Kits (Microsynth AG, Switzerland). The demultiplex raw reads (fastq) were used for gene expression analyses as described earlier [18]. In brief, the fastq files were used to align to human genome reference (GRCh38) using Hisat2, followed by transcripts assembly, and abundances estimation and differential expression were performed by cufflinks and cuffdiff, respectively. The visualization of RNAseq data analyses was performed by R packages, cummeRbund, gplots, and ggplot2 using customized scripts.

### Statistical Analysis

Statistical analysis of in vitro and in vivo differences in independent quantitative measures between every two treatment groups was performed using two-sided unpaired Student's *t* tests with Welch correction to protect against heteroscedastic data sets. In vitro comparisons for ABCB5<sup>+</sup> and donor-matched ABCB5<sup>-</sup> cell fractions were analyzed by a paired *t* test. On rare occasions, outliers detected by visual inspection of the data were excluded from the analysis after post hoc verification by the Grubbs' test at  $\alpha = 5\%$ . Statistical data analysis was done using GraphPad Prism 6 software (Software for Science). Graphs show mean, and error bars represent the standard deviation unless indicated otherwise and stars represent significance levels: ns = not significant; \*,  $p < .05$ ; \*\*,  $p < .01$ ; \*\*\*,  $p < .001$ .

## RESULTS

### Human and Murine Dermis Harbor ABCB5<sup>+</sup> Stromal Cells in the Perivascular and Interfollicular Niche

Using immunostaining of healthy human skin sections, we demonstrate that ABCB5<sup>+</sup> cells costain for the carbohydrate stage-specific embryonic antigen-4 (SSEA-4) (Fig. 1, 1B), an embryonic germ and stem cell marker [19] earlier reported to

be expressed on MSCs in different adult tissues, including the dermis [20–22].

Interestingly, ABCB5<sup>+</sup> cells either were confined to a perivascular endogenous niche, in close association with CD31<sup>+</sup> endothelial cells, or were dispersed within the interfollicular dermis independent of hair follicles (Fig. 1C). ABCB5<sup>+</sup> cells constituted  $2.45\% \pm 0.61\%$  of all dermal cells in the skin of 10 different donors and of the ABCB5<sup>+</sup> cells and  $55.3\% \pm 23.9\%$  were localized perivascularly, which was defined as a maximum of one additional cell in between the CD31<sup>+</sup> endothelial cell and the ABCB5<sup>+</sup> cell (Fig. 1D). Perivascular ABCB5<sup>+</sup> cells were distinct from neural/glial antigen 2 (NG2) positive pericytes [23], as there was almost no colocalization of NG2 with ABCB5 in double immunostained human skin sections (Fig. 1E, 1F). A similar distribution of ABCB5<sup>+</sup> cells in their endogenous niche was found in murine skin (Supporting Information Fig. S1).

Moreover, RNA sequence analysis from ABCB5<sup>+</sup>-enriched MSCs—even when expanded in culture to high passage numbers—revealed expression of distinct stemness as well as mesenchymal marker genes (Supporting Information Fig. S2A, S2B). Furthermore, we confirmed the expression of selected stemness markers such as SSEA-4, DPP4 (CD26), PRDM1 (BLIMP1), and POU5F1 (OCT-4) in ABCB5<sup>+</sup> cells in human skin at protein level by immunostaining (Supporting Information Fig. S2C–S2F), although the expression of lower fibroblast lineage marker  $\alpha$ -smooth muscle actin ( $\alpha$ -SMA) was absent in ABCB5<sup>+</sup> cells of human skin (Supporting Information Fig. S2G). Together these results support stemness properties of ABCB5<sup>+</sup> cells that are at least in part maintained in vitro and can be exploited therapeutically for the treatment of nonhealing wounds.

### Human Dermal ABCB5 Cells Reveal MSC Properties

To assess whether selection for ABCB5 results in a cell fraction with MSC properties, dermal single cell suspensions derived from enzymatically digested skin were separated by multiple rounds of ABCB5 magnetic bead sorting. This resulted in two different cell fractions, a double ABCB5-enriched fraction containing on average  $98.33\% \pm 1.12\%$  ABCB5<sup>+</sup> cells and a three-fold ABCB5-depleted fraction which only contained a very low percentage of ABCB5<sup>+</sup> cells as illustrated with flow cytometry dot plots for cells from donor B01 (Fig. 2A; Supporting Information Table S1A, S1B). Both ABCB5<sup>+</sup> and ABCB5<sup>-</sup> fractions displayed a fibroblastoid, spindle-like cell morphology (Fig. 2B) and expressed the characteristic minimal set of mesenchymal lineage markers CD90, CD105, and CD73, whereas no expression of hematopoietic stem cell and lineage markers CD34, CD14, CD20, and CD45 [24] was detected by flow cytometry (Fig. 2C). A consistent and significantly increased potential for adipogenic, osteogenic, and chondrogenic lineage differentiation was observed for ABCB5<sup>+</sup> cells as compared with donor-matched ABCB5-depleted cells (Fig. 2D–2F), thereby delineating the ABCB5<sup>+</sup> fractions as multipotent adult MSCs from ABCB5<sup>-</sup> HDFs. This was further confirmed by the finding that ABCB5<sup>+</sup> sorted cells gave rise to single-cell-derived colonies, whereas the ABCB5-depleted fractions did not (Fig. 2G). To assess the in vitro self-renewal capacity of dermal ABCB5<sup>+</sup>-derived MSCs, subclonogenic growth and trilineage differentiation potential of 54 clonal cultures of ABCB5<sup>+</sup>-sorted MSCs from six different donors were determined (Fig. 2H). Interestingly,  $75.61\% \pm 16.86\%$  of clonal colonies again displayed clonogenic growth and  $62.40\% \pm 7.54\%$  of all studied clones, generated from a



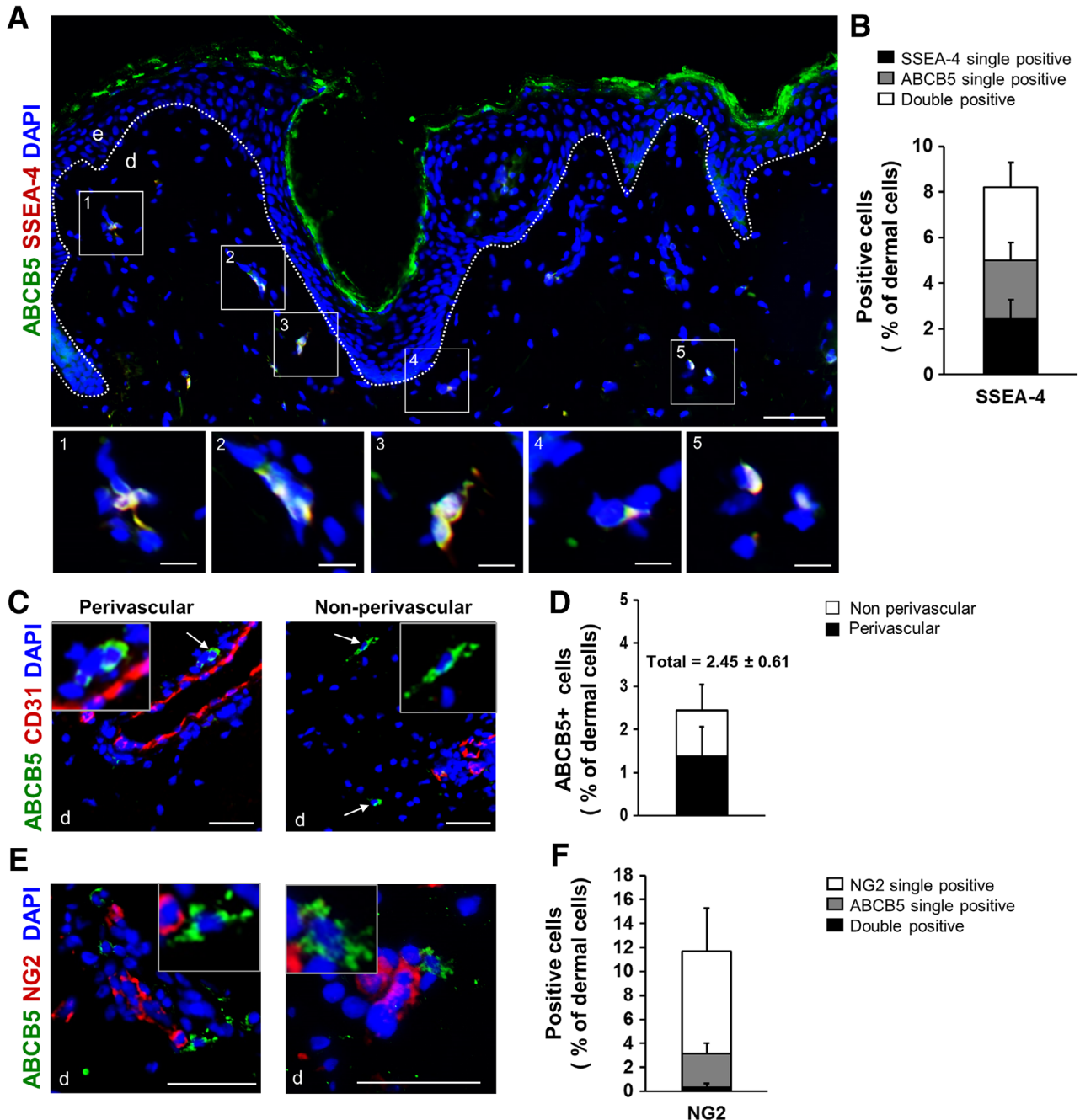


**Figure 1.** In situ characterization of ABCB5<sup>+</sup> cells in their endogenous niche in healthy human skin. **(A, B):** A microphotographic overview of healthy human skin subjected to immunostaining for ABCB5 (green) and the adult stem cell marker SSEA4 (red) revealed a distinct subpopulation of dermal cells positive for both markers (yellow overlay). Quantification of ABCB5 positive and SSEA-4 positive proved that 94.39% of dermal cells expressing ABCB5 were copositive for SSEA-4. **(C):** Microphotographs of human skin subjected to immunostaining for ABCB5 (green) and the endothelial marker CD31 (red) revealed both a perivascular (left) and a dispersed interfollicular dermal localization (right) of ABCB5<sup>+</sup> cells (white arrows), whereas no colocalization of ABCB5 and CD31 was observed. **(D):** ABCB5<sup>+</sup> cells occurred at an average percentage of  $2.45 \pm 0.61$  of all dermal cells as determined in 8–10 microscopic fields of skin sections from 10 different donors. ABCB5<sup>+</sup> cells were more abundant in a perivascular localization compared with a nonperivascular localization. **(E):** Double immunofluorescence staining for ABCB5 (green) and the pericyte marker NG2 (red) shows that perivascular ABCB5<sup>+</sup> cells (white arrows) are distinct from NG2<sup>+</sup> pericytes. **(F):** Quantification of ABCB5 positive and NG2 positive depict that only 0.32% of total dermal cells coexpressed ABCB5 and NG2 as determined in more than 20 microscopic fields of skin sections from five different donors. **(A, B, D):** Nuclei of all studied skin sections were counterstained with DAPI (blue). Scale bars = 50  $\mu$ m; e = epidermis; d = dermis. Dashed white lines delineate epidermal from dermal layers. Abbreviations: ABCB5, ATP-binding cassette subfamily B member 5; DAPI, 4',6-diamidino-2-phenylindole; NG2, neural/glial antigen 2; SSEA-4, stage-specific embryonic antigen-4.

single cell, maintained their potential to differentiate into all three mesenchymal cell lineages (Fig. 2H). An additional  $29.84\% \pm 11.57\%$  of these clones were bipotent and

$7.77\% \pm 10.02\%$  were unipotent for osteogenic differentiation (Fig. 2H). None of the clones from six donors were negative for all three lineages. When compared with the gold-

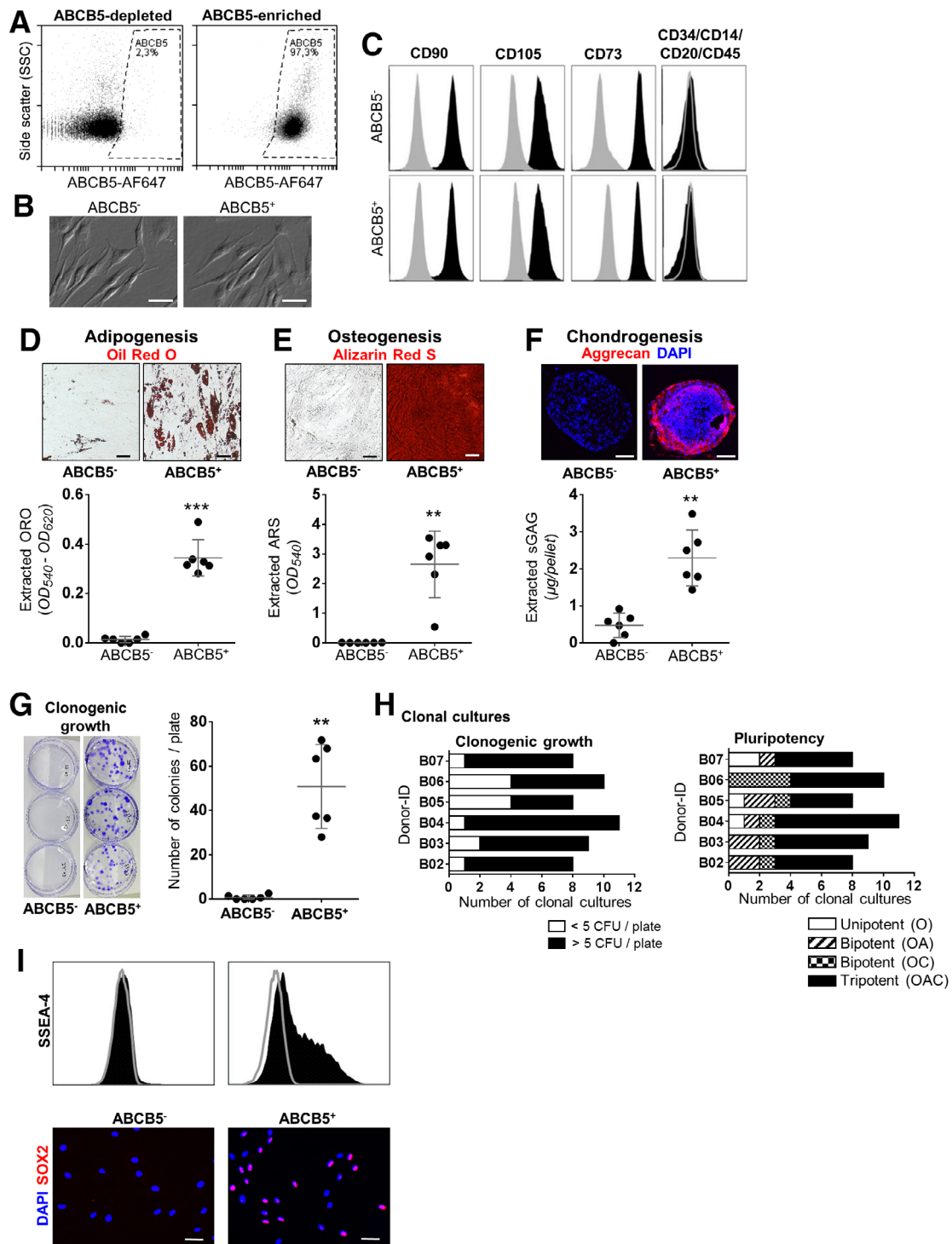


**Figure 2.** In vitro characterization of ABCB5<sup>+</sup> dermal cells. **(A):** Flow cytometry reproducibly confirmed high purity of ABCB5<sup>+</sup> and ABCB5<sup>-</sup> dermal cell fractions. **(B):** Differential interference contrast micrographs depict a fibroblast-like phenotype for both ABCB5<sup>+</sup> and ABCB5<sup>-</sup> fractions. **(C):** Flow cytometry results show that both fractions expressed CD90, CD73, and CD105 and lacked CD14, CD20, CD34, and CD45 expression (black). Gray histograms represent isotope controls. **(D–F):** in vitro trilineage differentiation was more prominent for ABCB5<sup>+</sup> than for ABCB5-depleted dermal cells. Adipogenic and osteogenic differentiation was quantified by extraction of respective ORO **(D)** and ARS **(E)** indicator dyes. Chondrogenic differentiation **(F)** was visualized by aggrecan immunostaining (red) and quantitatively assessed by extraction of sGAG. **(G):** Following low-density seeding, only cells from ABCB5<sup>+</sup>-sorted fractions formed crystal violet-visualized colonies. **(H):** ABCB5<sup>+</sup>-sorted cell clonal cultures were subjected to a second CFU assay and tri-lineage (O = osteogenic; A = adipogenic; C = chondrogenic) differentiation. Threshold for clonogenic growth (five colonies) and positive differentiation was set 3 SD above the average from ABCB5<sup>-</sup> samples or unstimulated controls, respectively. **(I):** SSEA-4<sup>+</sup> cells by flow cytometry and SOX2<sup>+</sup> nuclei (red) by immunofluorescence staining were found exclusively within ABCB5<sup>+</sup> fractions. Nuclei are counterstained with DAPI (blue). Scale bars = 50 µm. \*\*, *p* < .01; \*\*\*, *p* < .001, *t* test. Abbreviations: ABCB5, ATP-binding cassette subfamily B member 5; CFU, colony-forming unit; DAPI, 4',6-diamidino-2-phenylindole; sGAG, sulfated glycosaminoglycans; SSEA-4, stage-specific embryonic antigen-4; ORO, Oil Red O; ARS, Alizarin Red S; SSC, Side scatter.

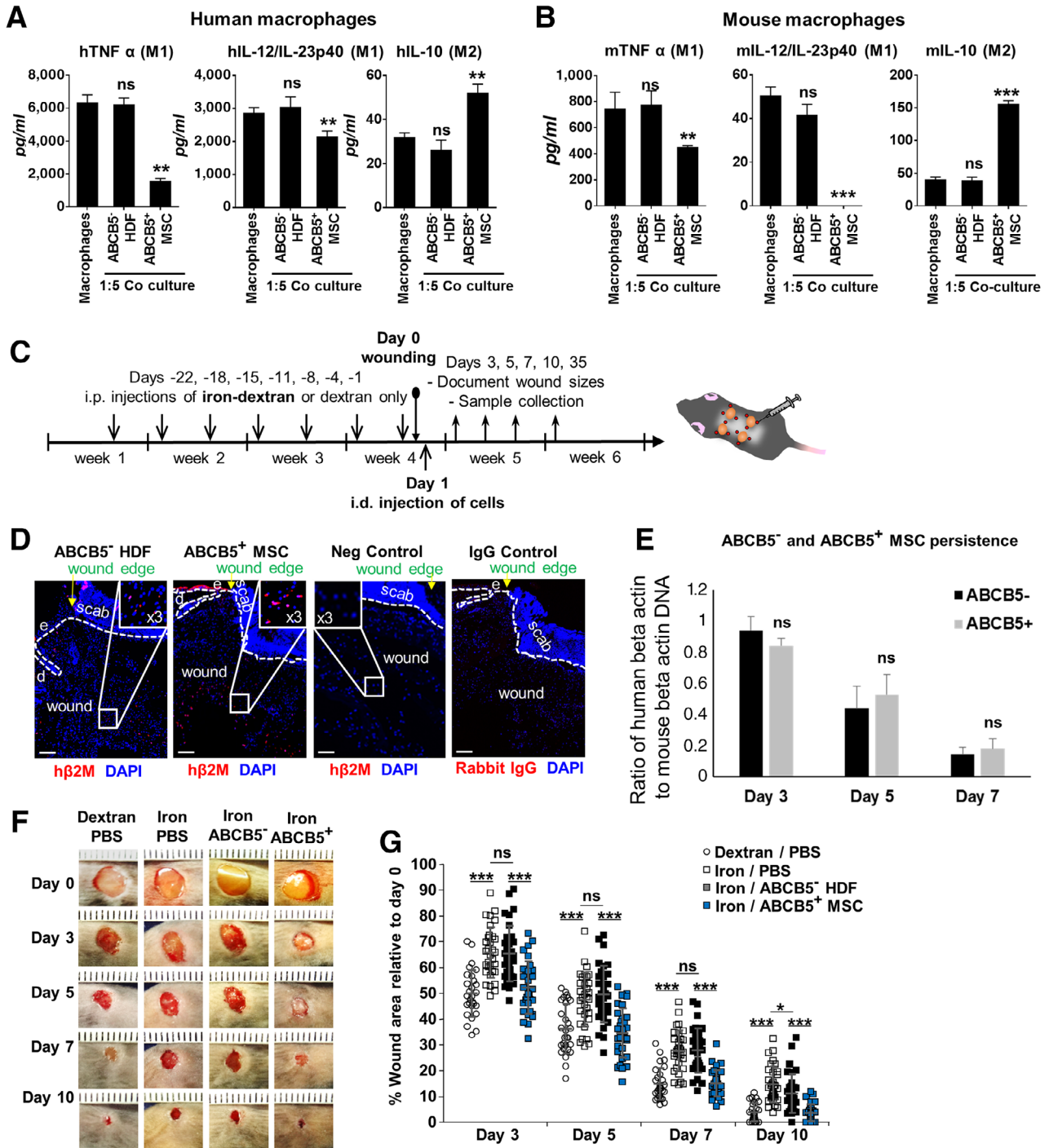


**Figure 3.** Human ABCB5<sup>+</sup>-derived MSCs accelerate impaired wound healing by inducing a switch from classically activated M1 to regenerative M2 macrophages. **(A):** Coculture of human dermal ABCB5<sup>+</sup>-derived MSC with human macrophages matured from peripheral blood monocytes at a ratio of 1:5 significantly downregulates the secretion of the proinflammatory M1 cytokines TNFα (left) and IL-12/IL-23p40 (middle) upon classical IFN-γ/LPS activation as measured by enzyme-linked immunosorbent assay. The anti-inflammatory M2 cytokine IL-10 (right) was upregulated upon ABCB5<sup>+</sup>-derived MSC macrophage coculture. By contrast, donor-matched ABCB5<sup>-</sup> HDFs did not show any change in cytokine release when cocultured with activated macrophages. **(B):** In a cross-species, 1:5 coculture setting of human dermal ABCB5<sup>+</sup>-derived MSCs or donor-matched ABCB5<sup>-</sup> HDFs, respectively, with mouse macrophages revealed similar results as in **(A)**. **(C):** Scheme depicting the timeline for the iron-overload mouse model used. Intraperitoneal iron-dextran injections and intradermal injections into wound edges were performed as illustrated. **(D):** Persistence and localization of ABCB5<sup>-</sup> cells and ABCB5<sup>+</sup>-derived MSCs within the wound bed at day 3 was visualized by immunostaining for human β2M (red). The negative control showing immunostaining of a section of a mouse wound in the absence of any human-derived MSCs injections. Scale bars = 100 μm; e = epidermis; d = dermis. Dashed white lines delineate epidermal from dermal layers. Nuclei were DAPI counterstained (blue). **(E):** ABCB5<sup>+</sup> MSCs and ABCB5<sup>-</sup> MSCs were detected and quantified in wounds at indicated time points postwounding by human beta actin sequence polymerase chain reaction; ns, nonsignificant. **(F):** Ruler-assisted size-equalized wound pictures representative for defined interventions at the indicated time points after wounding. **(G):** Quantification (Figure legend continues on next page.)

standard of bone marrow-derived MSCs with a trilineage differentiation capacity of 34% in more than 200 studied single-cell clones [25], the trilineage differentiation capacity >70% was apparently better in ABCB5<sup>+</sup> skin-derived MSCs.

In contrast to triple ABCB5-depleted cells, the ABCB5<sup>+</sup>-sorted cell fractions revealed distinct stem-cell-associated SSEA-4 [26] expression (Fig. 2I). This matches with the observed coexpression of ABCB5<sup>+</sup> cells with SSEA-4 in human skin (Fig. 1A). Nuclei of ABCB5<sup>+</sup> cells grown on slides stained positive for SOX2, the stem-cell-associated transcription factor sex determining region Y-box 2, whereas ABCB5<sup>-</sup> cells did not (Fig. 2I). Neither ABCB5<sup>+</sup> nor ABCB5<sup>-</sup> dermal plastic-adherent cell fractions expressed the additionally tested cell surface markers Melan-A (melanocytic cells), CD133 (cancer stem cells), CD318 (epithelial cells), and CD271 (a neurotrophic factor found on other MSC populations; Supporting Information Fig. S3).

### Human ABCB5<sup>+</sup>-Derived MSCs Accelerate Wound Healing in Iron-Overload Mice Through Triggering a Switch from M1 to M2 Macrophages

In order to address whether the here characterized dermal ABCB5<sup>+</sup>-derived MSCs exert anti-inflammatory effects on classically activated M1 macrophages, ABCB5<sup>+</sup>-derived MSCs were cocultured with allogeneic PBMC CD14<sup>+</sup> monocyte-derived macrophages that had been activated with recombinant human IFN- $\gamma$  and LPS (Fig. 3A). Of note, significantly less M1 macrophage-derived proinflammatory cytokines TNF $\alpha$  and IL-12/IL-23p40 were detected in supernatants when activated macrophages were cocultured with ABCB5<sup>+</sup>-derived MSCs, as opposed to cocultures with donor-matched ABCB5<sup>-</sup> HDFs or macrophages cultured alone. Conversely, increased amounts of IL-10, a M2 macrophage-derived anti-inflammatory cytokine, were found in supernatants of macrophages cocultured with ABCB5<sup>+</sup>-derived MSCs as opposed to donor-matched ABCB5<sup>-</sup> HDFs or macrophages cultured alone (Fig. 3A). Of note, pooled ABCB5<sup>+</sup>-derived MSCs from six different donors revealed a similar suppressive action on M1 macrophage cytokines with a concomitant upregulation of the M2 macrophage cytokine IL-10 when compared with the single ABCB5<sup>+</sup>-derived MSCs (Supporting Information Fig. S4). These data imply that pooled preparations of ABCB5<sup>+</sup>-derived MSCs would be a practically relevant option for the treatment of nonhealing wounds in clinical routine.

Similar to cocultures of human ABCB5<sup>+</sup>-derived MSCs with human macrophages, human ABCB5<sup>+</sup>-derived MSCs exert identical effects on murine macrophages in a cross-species setting (Fig. 3B; Supporting Information Fig. S4), thereby confirming functional relevance for subsequent wound healing studies in a murine xenograft model.

Next, in order to specifically investigate the paracrine effects of ABCB5<sup>+</sup>-derived MSCs on suppression of M1 macrophages, which—due to their unrestrained activation—are responsible for the nonhealing state of chronic human wounds, we used the iron-overload mouse model [7] with full-thickness excisional wounds in a xenograft setting. The iron-overload wound

model faithfully recapitulates major pathogenic aspects of chronic venous leg ulcers [7]. ABCB5<sup>+</sup>-derived and ABCB5-depleted dermal human cells were injected into the dermis around the wound edges at day 1 after wounding as graphically depicted (Fig. 3C). The persistence of injected human cells at day 3 after wounding was confirmed by immunostaining for the human major histocompatibility complex I constant subunit  $\beta$ 2-microglobulin ( $\beta$ 2M) (Fig. 3D). By means of human-specific beta actin sequence PCR on genomic DNA isolated from wound sections, we confirmed persistence of human-specific beta actin-signals to a similar extent in the wounds injected with either ABCB5<sup>+</sup>-derived MSCs or ABCB5<sup>-</sup> cells at indicated time points (Fig. 3E). Therefore, differences in the persistence between ABCB5<sup>+</sup> and ABCB5<sup>-</sup> cells did not confound our results.

We next addressed the question whether injection of ABCB5<sup>+</sup>-derived MSCs accelerate wound closure in the iron-overload model. As expected, we observed delayed wound closure in iron-treated/PBS-injected mice as compared with dextran-treated/PBS-injected control mice (Fig. 3F, 3G). Of note, a significantly accelerated wound closure was observed after intradermal injection of 10<sup>6</sup> ABCB5<sup>+</sup>-derived MSCs around four wounds (per mouse) compared with injection of donor-matched ABCB5<sup>-</sup> HDFs or PBS alone (Fig. 3F, 3G). Treatment with ABCB5<sup>+</sup>-derived MSCs fully restored the wound closure rate to that of dextran-treated/PBS-injected control mice (Fig. 3F, 3G). Together these findings suggest beneficial effects of ABCB5<sup>+</sup>-derived MSCs for the cure of nonhealing chronic wounds.

### Human ABCB5<sup>+</sup>-Derived MSCs Suppress Inflammation and Improve all Subsequent Wound Phases in Iron-Overload Mice

Chronic wounds persist in the inflammatory wound phase with unrestrained M1 macrophage activation and fail to progress through the normal phases of wound healing. We here studied whether injection of ABCB5<sup>+</sup>-derived MSCs may suppress the unrestrained M1 macrophage-dependent inflammation and allow the wounds to follow the normal sequence of different wound phases. Employing double immunostaining, we found ABCB5<sup>+</sup>-derived MSCs in close association to endogenous murine macrophages when injected in iron-overload wounds (Supporting Information Fig. S5), implying that a paracrine effect of ABCB5<sup>+</sup>-derived MSCs on macrophages is possible in wound tissue. In a first attempt to explore a paracrine impact of ABCB5<sup>+</sup>-derived MSCs on macrophage-dominated inflammation in iron-overload wounds, whole wound cytokine profiles were studied by ELISA on protein lysates (Fig. 4A). Notably, at day 5 after wounding, wound tissue protein levels of the inflammatory cytokine TNF $\alpha$  were dampened (Fig. 4A), whereas anti-inflammatory IL-10 was increased in iron-overload wounds injected with ABCB5<sup>+</sup>-derived MSCs but not with ABCB5<sup>-</sup> HDF controls (Fig. 4A). Furthermore, the inflammatory cytokine IL-1 $\beta$ , that is typically upregulated in human CVU (Supporting Information Fig. S6A, S6C) and in iron-overload murine model (Supporting Information Fig. S6B, S6D),

(Figure legend continued from previous page.)

of wound areas depicted in (F) relative to day 0 confirmed delayed wound closure in the iron-model (open squares) compared with dextran-injected control wounds (open circles). Wound healing delay in the iron-model was rescued by ABCB5<sup>+</sup>-derived MSCs (blue squares) but not by ABCB5<sup>-</sup> HDFs (black squares). ns = not significant; \*,  $p < .05$ ; \*\*,  $p < .01$ ; \*\*\*,  $p < .001$ ,  $t$  test. Abbreviations: ABCB5, ATP-binding cassette subfamily B member 5; DAPI, 4',6-diamidino-2-phenylindole; HDF, human dermal fibroblasts; IL, interleukin; MSC, mesenchymal stem cells; PBS, phosphate-buffered saline; TNF $\alpha$ , tumor necrosis factor alpha.

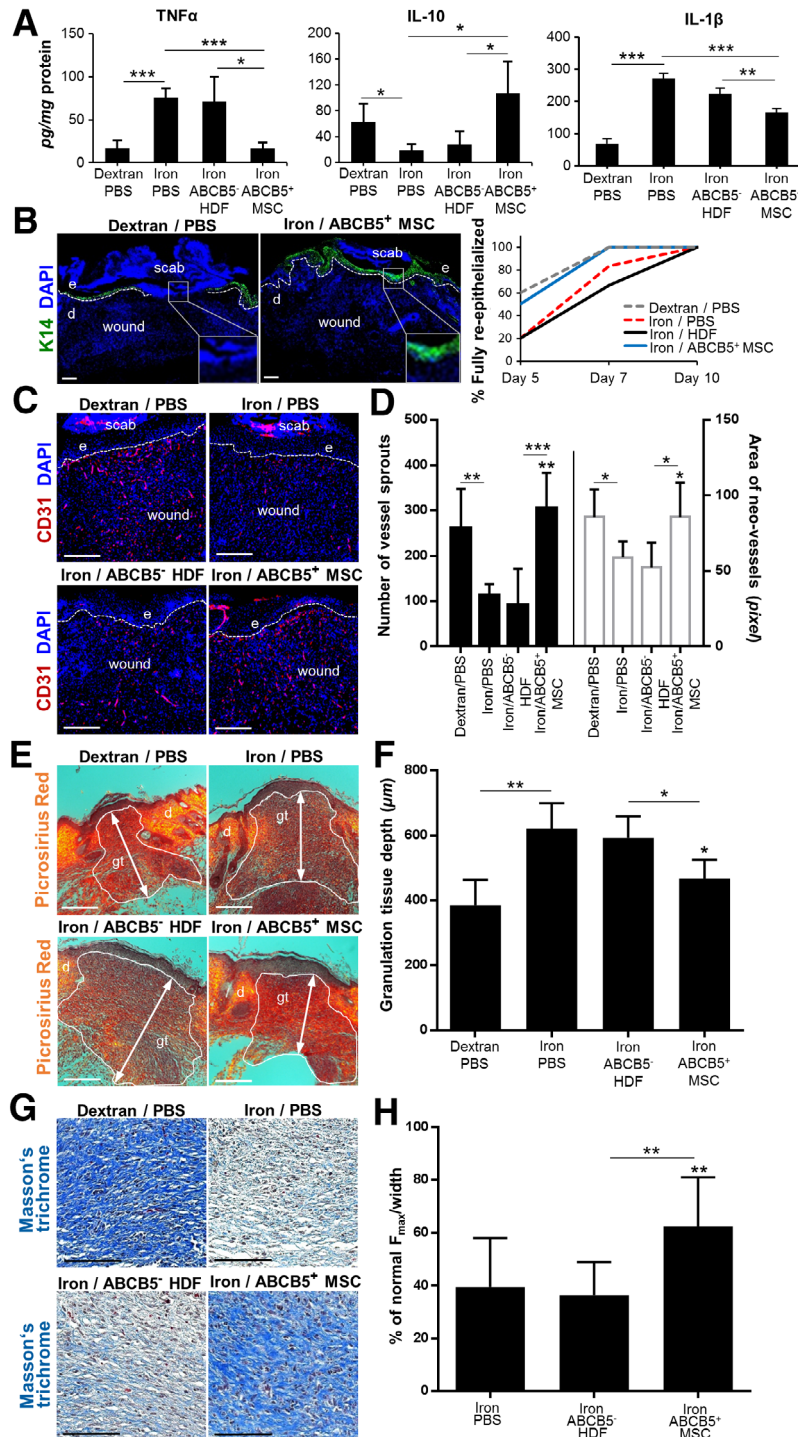


**Figure 4.** ABCB5<sup>+</sup> MSCs rescue imbalanced wound healing in iron-overload mice. **(A):** Opposed to ABCB5<sup>-</sup>-derived HDFs, ABCB5<sup>+</sup>-derived MSC suppressed M1 cytokines (TNF $\alpha$ , IL-1 $\beta$ ), whereas increased M2-associated IL-10 (assessed by ELISAs) ( $n = 4$ ). **(B):** Keratin14 immunostaining (green) illustrates incomplete (left) and complete (middle) re-epithelialization. Percentages of re-epithelialized wounds over treatment groups (right) indicate faster epithelial closure upon ABCB5<sup>+</sup>-derived MSC treatment (blue) as compared with PBS (dashed red) or ABCB5<sup>-</sup> HDFs controls (black). **(C):** Impaired neoangiogenesis in the iron-overload wound model, assessed by CD31 immunostaining (red), was fully rescued with ABCB5<sup>+</sup>-derived MSC supplementation. **(D):** Number and size of CD31<sup>+</sup> vessel sprouts confirmed this ( $n = 6$ ). **(E):** Picrosirius red histology indicated advanced matrix constitution of the outlined granulation tissue (gt) with more collagen fibers (yellow-red birefringence) following ABCB5<sup>+</sup>-derived MSC treatment. **(F):** Reduced gt thickness (white arrows in E) was found for ABCB5<sup>+</sup>-derived MSC-injected wounds when compared with iron-model controls. **(G):** Masson trichrome illustrates densely woven collagen matrix proteins (blue) following ABCB5<sup>+</sup>-derived MSC injection, comparable to acute wounds. Scale bars = 100  $\mu\text{m}$ . **(H):** Scar tensile strength was significantly improved in ABCB5<sup>+</sup>-derived MSC-injected iron-overload wounds. **(B, C, E):** Scale bars = 200  $\mu\text{m}$ ; e = epidermis; d = dermis. Dashed lines delineate epidermis from dermis. Nuclei were DAPI-counterstained (blue) **(B, C)**. \*,  $p < .05$ ; \*\*,  $p < .01$ ; \*\*\*,  $p < .001$ ,  $t$  test. Abbreviations: ABCB5, ATP-binding cassette subfamily B member 5; DAPI, 4',6-diamidino-2-phenylindole; HDF, human dermal fibroblasts; IL, interleukin; MSC, mesenchymal stem cells; PBS, phosphate-buffered saline; TNF $\alpha$ , tumor necrosis factor alpha.

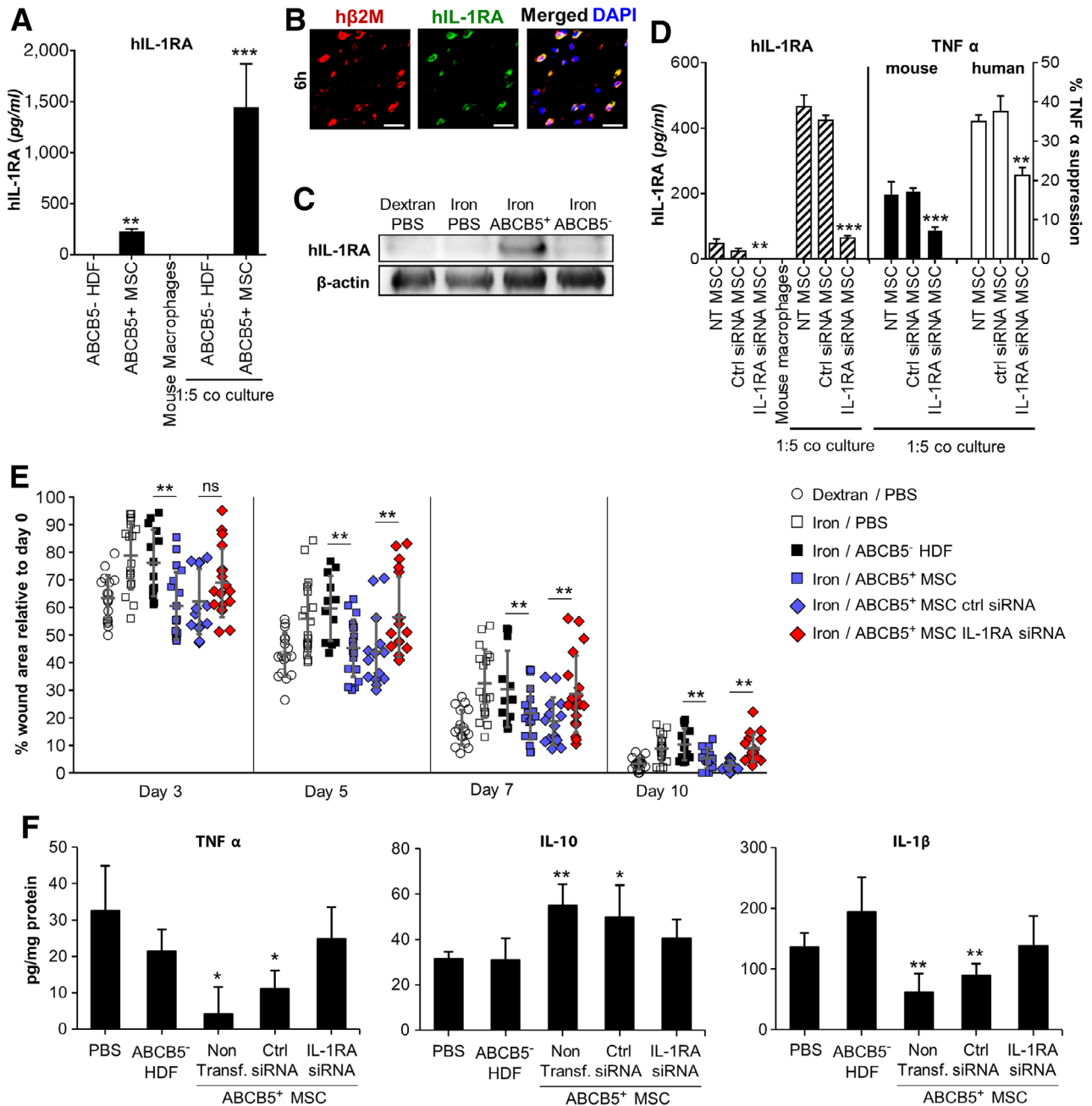


**Figure 5.** ABCB5<sup>+</sup>-derived MSCs rescue delayed wound healing via IL-1RA secretion. **(A):** ABCB5<sup>+</sup>-MSCs cultured alone (black bars) or with murine macrophages, secreted IL-1RA following IFN-γ/LPS stimulation, whereas ABCB5<sup>-</sup> HDFs did not. **(B):** Production of human IL-1RA<sup>+</sup> (green) by β2M<sup>+</sup> (red) human ABCB5<sup>+</sup>-derived MSCs was observed 6 hours after ABCB5<sup>+</sup> MSCs injection around iron-overload wounds. Scale bars = 50 μm. **(C):** A ~22 kDa band for lysates of three pooled ABCB5<sup>+</sup>-derived MSCs-injected day 3 wounds, but not in ABCB5<sup>-</sup> HDF-injected wounds, was detected by human IL-1RA-specific immunoblotting. **(D):** IL-1RA silencing in ABCB5<sup>+</sup>-derived MSCs abrogated adaptive upregulation of IL-1RA (hatched bars) and significantly diminished TNFα suppression in activated murine (black bars) and human (white bars) macrophages in corresponding cocultures. **(E):** Rescued wound healing and decreased wound areas following ABCB5<sup>+</sup>-derived MSC injection (blue squares) in iron-overload mice was almost completely abrogated in IL-1RA siRNA (red diamonds) but not control siRNA transfected ABCB5<sup>+</sup>-derived MSCs (blue diamonds) from day 5 wounds onward. **(F):** Day 5 proinflammatory cytokine profiles of iron-overload wounds remained unaltered when IL-1RA silenced ABCB5<sup>+</sup>-derived MSCs had been injected. **(A, D, F):** Bar graphs represent ELISA results. Significance level indications relate to control activated macrophages alone **(A)**, respective siRNA-transfected groups **(D)** and PBS-treated group **(F)**. \*, *p* < .05; \*\*, *p* < .01; \*\*\*, *p* < .001, *t* test. Abbreviations: ABCB5, ATP-binding cassette subfamily B member 5; DAPI, 4',6-diamidino-2-phenylindole; HDF, human dermal fibroblasts; IL, interleukin; IL-1RA, interleukin-1 receptor antagonist; MSC, mesenchymal stem cells; PBS, phosphate-buffered saline; TNFα, tumor necrosis factor alpha.

was significantly suppressed upon treatment with ABCB5<sup>+</sup>-derived MSCs (Fig. 4A, right panel).

We also observed faster re-epithelialization with a fully restored K14<sup>+</sup> epithelial cell layer covering the entire wound bed, a key

feature of successful skin repair, in day 7 iron-overload wounds when injected with ABCB5<sup>+</sup>-derived MSCs as opposed to ABCB5<sup>-</sup> HDF-injected wounds (Fig. 4B). We observed a significant improvement of neovascularization (Fig. 4C) as confirmed by increased

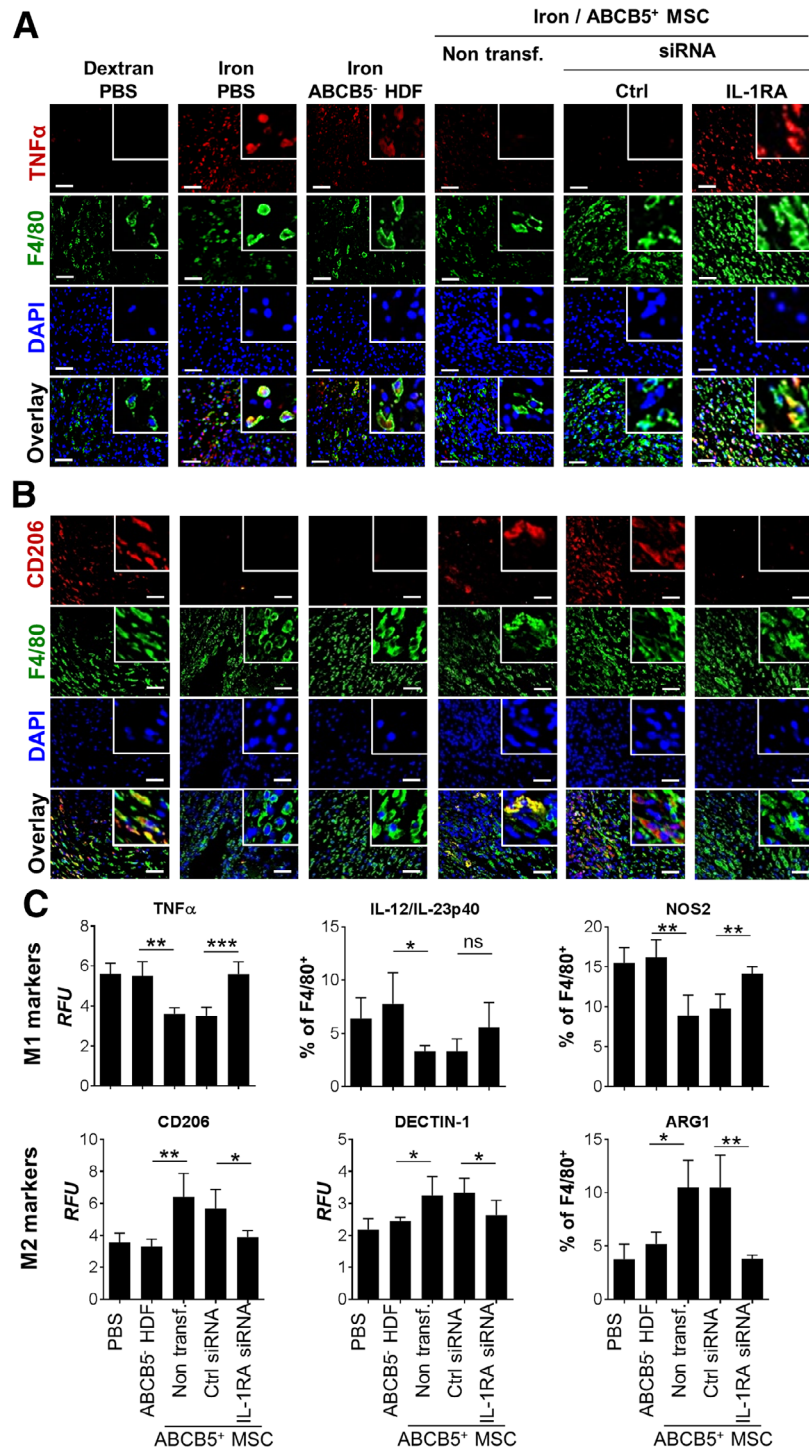


**Figure 6.** ABCB5<sup>+</sup>-derived MSCs mediate a shift from M1 to anti-inflammatory M2 wound macrophages via IL-1RA. **(A):** Representative microphotographs of double immunostaining for macrophage F4/80 (green) and murine TNFα (red) in skin sections of day 5 wounds illustrate reduction of M1 macrophages following injection with ABCB5<sup>+</sup>-derived MSCs but not ABCB5<sup>-</sup> HDFs at the wound margins. This M1 macrophage suppressive effect was abrogated when IL-1RA silenced ABCB5<sup>+</sup> MSCs were injected. **(B):** Double immunostaining for F4/80 (green) and the M2 marker CD206 (red) displayed an IL-1RA-dependent increase in M2 macrophages in iron-overload wounds, comparable to M2 macrophage numbers in physiological wound healing controls (Dextran/PBS) at day 5 postwounding. **(A, B):** Scale bars = 50 μm; inserts are three-fold enlarged. Nuclei are stained with DAPI (blue). **(C):** Multi-color flow cytometry on singlet F4/80<sup>+</sup> wound single cell preparations at day 5 postwounding confirm a wound macrophage immune-phenotype shift with downregulation of M1 markers like TNFα, IL-12/IL-23p40, and NOS2 and upregulation of the M2 markers CD206, Dectin-1, and ARG1 IL-1RA-dependently mediated by ABCB5<sup>+</sup> MSCs but not by donor-matched ABCB5<sup>-</sup> HDFs. ns = not significant; \*, *p* < .05; \*\*, *p* < .01; \*\*\*, *p* < .001, *t* test. Abbreviations: ABCB5, ATP-binding cassette subfamily B member 5; DAPI, 4',6-diamidino-2-phenylindole; HDF, human dermal fibroblasts; IL, interleukin; IL-1RA, interleukin-1 receptor antagonist; MSC, mesenchymal stem cells; PBS, phosphate-buffered saline; TNFα, tumor necrosis factor alpha.

number and area of CD31<sup>+</sup> vessel sprouts within the wound bed at day 7 (Fig. 4D). In addition, injection of ABCB5<sup>+</sup>-derived MSCs in wound edges of iron-overload mice markedly improved the tissue remodeling with increased maturation of collagen fibers (Fig. 4E), reduced granulation tissue depth (Fig. 4F), and improved organization of collagen fibers in more densely basket-woven fibrillary structure (Fig. 4G). Of note, iron-overload wounds injected with ABCB5<sup>+</sup>-derived MSCs depicted a significantly higher tensile strength of the scar tissue, a strong indication for improved quality of the restoration tissue, as compared with less tensile strength in scar tissue of ABCB5<sup>-</sup> HDF or PBS-treated iron-overload wounds (Fig. 4H). These data show that ABCB5<sup>+</sup>-derived MSCs positively impact on several wound healing phases and not only accelerate tissue repair but importantly lead to a scar-reduced, quality-improved restoration tissue.

### ABCB5<sup>+</sup>-Derived MSCs Suppress Macrophage-Dominated Inflammation via Adaptive Secretion of IL-1RA

Given the abundance of IL-1 $\beta$  and its inflammation amplifying effector TNF $\alpha$  [7] in chronic wounds as opposed to transiently induced low IL-1 $\beta$  concentrations in acute wounds, we addressed the question as to whether human dermal ABCB5<sup>+</sup>-derived MSCs are able to produce the natural antagonist of IL-1 signaling, IL-1RA. We found that unstimulated ABCB5<sup>+</sup>-derived MSCs in culture did not readily produce IL-1RA as assessed by a specific ELISA (Fig. 5A). However, in contrast to donor-matched ABCB5<sup>-</sup> HDFs, ABCB5<sup>+</sup>-derived MSCs released high IL-1RA levels when stimulated with IFN- $\gamma$  /LPS (Fig. 5A). Of note, the IL-1RA concentration was even higher in cocultures of ABCB5<sup>+</sup>-derived MSCs with IFN- $\gamma$ /LPS-activated M1 macrophages (Fig. 5A). Six hours after injection, specific IL-1RA expression was observed in ABCB5<sup>+</sup>-derived MSCs at the wound site of iron-overload mice as shown by double immunostaining with distinctly colocalized human-specific  $\beta$ 2M and IL-1RA (Fig. 5B). Employing Western blot analysis, we confirmed high IL-1RA expression in pooled day 3 wound lysates prepared from iron-overload ABCB5<sup>+</sup>-derived MSCs-injected wounds as compared with no IL-1RA expression in ABCB5<sup>-</sup> HDFs or in PBS-injected control wound lysates (Fig. 5C). Of note, and previously unreported, we also observed IL-1RA expression in endogenous murine ABCB5<sup>+</sup> MSCs in iron-overload model wound healing, whereas in healthy skin, neither murine nor human endogenous ABCB5<sup>+</sup>-derived MSCs were found to express IL-1RA (Supporting Information Fig. S7). These data imply an adaptive production of IL-1RA by dermal ABCB5<sup>+</sup> MSCs in response to the inflammatory environment of iron-overload wounds. A small fraction of murine macrophages, but not neutrophils, release IL-1RA in iron-overload chronic wounds (Supporting Information Fig. S8). The therapeutic impact of IL-1RA released from ABCB5<sup>+</sup>-derived MSCs on acceleration of healing of iron-overload wounds is, however, significantly more important, as IL-1RA-silenced MSCs, when injected into iron-overload wounds, cannot restore delayed wound healing. We next explored whether IL-1RA released by ABCB5<sup>+</sup>-derived MSCs are responsible for the suppression of M1 macrophage-derived TNF $\alpha$  in vitro and in vivo. ABCB5<sup>+</sup>-derived MSCs were assessed for TNF $\alpha$  release in wounds supernatants of iron-overload mice injected with either IL-1RA silenced or competent ABCB5<sup>+</sup>-derived MSCs. Notably, silencing of IL-1RA in ABCB5<sup>+</sup>-derived MSCs at least partially abrogated TNF $\alpha$  suppression in cocultures with either human or murine macrophages (Fig. 5D). As expected, scrambled control siRNA transfected IL-1RA competent control ABCB5<sup>+</sup>-derived MSCs

revealed their full suppressive effect on TNF $\alpha$  release from activated macrophages in vitro (Fig. 5D). Strikingly, intradermal injection of IL-1RA silenced ABCB5<sup>+</sup>-derived MSCs into wound edges of iron-overload mice resulted in a complete loss of accelerated wound closure (Fig. 5E). By contrast, scrambled siRNA transfected IL-1RA competent ABCB5<sup>+</sup> MSCs maintained their capacity to accelerate wound healing at the indicated time points in vivo (Fig. 5E). The loss of the capacity of IL-1RA silenced ABCB5<sup>+</sup> MSCs to accelerate healing in iron-overload wounds was associated with a reversal of TNF $\alpha$  and IL-1 $\beta$  suppression and IL-10 upregulation (Fig. 5F). These data indicate that IL-1RA adaptively released from ABCB5<sup>+</sup> MSCs upon stimulation at the wound site not only suppresses IL-1 signaling but also the downstream effector TNF $\alpha$  and, importantly, even induces anti-inflammatory IL-10. The notion that IL-1RA released from ABCB5<sup>+</sup>-derived MSCs at the wound site suppressed unrestrained M1 activation with improved wound healing is further supported by our finding that intradermal injection of recombinant human IL-1RA around iron-overload wounds also accelerated wound closure (Supporting Information Fig. S9A). By contrast, injection of recombinant IL-1RA into acute wounds did not accelerate healing (Supporting Information Fig. S9B). We also found tumor necrosis factor-inducible gene 6 (TSG-6) to be expressed in ABCB5 human MSCs in iron-overload wounds (Supporting Information Fig. S10A, S10B). However, when injecting recombinant TSG-6 into iron-overload wounds, no improvement of wound closure occurred (Supporting Information Fig. S10C). Our results imply that IL-1RA, indeed, plays a central role in iron-overload wounds, whereas recombinant human TSG-6 alone is not sufficient to accelerate healing in the iron-overload situation. This implies that different wound types reveal distinct requirements for therapeutic acceleration of their healing.

### ABCB5<sup>+</sup>-Derived MSCs Break M1 Macrophage Persistence in Wounds of Iron-Overload Mice

To further sustain the hypothesis that wound treatment with ABCB5<sup>+</sup>-derived MSC would IL-1RA-dependently break the prolonged persistence of M1 macrophages in wounds of the iron-overload mice, a series of double immunostainings of day 5 wound sections were performed. In fact, TNF $\alpha$  expressing F4/80<sup>+</sup> macrophages were virtually absent in iron-overload wounds injected with ABCB5<sup>+</sup>-derived MSCs (Fig. 6A). In stark contrast, many TNF $\alpha$ <sup>+</sup> F4/80<sup>+</sup> double positive macrophages persisted in wound margins upon injection of IL-1RA silenced ABCB5<sup>+</sup>-derived MSCs similar to dextran pretreated acute healing control mice (Fig. 6A). These data indicate that ABCB5<sup>+</sup>-derived MSCs IL-1RA-dependently suppress wound macrophage released TNF $\alpha$  production in vivo. Interestingly, CD206<sup>+</sup> F4/80<sup>+</sup> wound healing-promoting M2 macrophages appeared to be IL-1RA-dependently enriched in ABCB5<sup>+</sup>-derived MSCs-injected wounds at day 5 postwounding (Fig. 6B). In fact, immune phenotyping of single cell preparations of day 5 wounds injected with ABCB5<sup>+</sup>-derived MSCs (Supporting Information Fig. S11A) quantitatively confirmed an IL-1RA-dependent switch of inflammatory M1 toward wound healing-promoting M2 macrophages as defined by distinct sets of surface markers (Fig. 6C). Thus, M1 activation markers, including cytokines (TNF $\alpha$  and IL-12/IL-23p40) and the inducible nitric oxide synthase (NOS2) were downregulated and M2 activation markers like the mannose receptor CD206, the  $\beta$ -glycan Dectin-1, and arginase-1 (ARG1) were upregulated in F4/80<sup>+</sup> wound macrophages after ABCB5<sup>+</sup>-derived MSCs injection (Fig. 6C). This M1 to M2 shift was



maintained in scrambled siRNA transfected ABCB5<sup>+</sup>-derived MSCs, whereas it was almost completely abrogated following injection with IL-1RA siRNA transfected ABCB5<sup>+</sup>-derived MSCs (Fig. 6C, outer right lower panel). In aggregate, these results uncover a causal role for IL-1RA to abrogate persistence of M1 macrophage in chronic wounds secreted by ABCB5<sup>+</sup>-derived MSCs.

### The ABCB5<sup>+</sup>-Derived MSCs-Dependent M1 to M2 Macrophage Shift Is Conserved in Humanized NSG Mice

NSG mice, humanized with PBMC, represent a highly suitable preclinical model to investigate effects of therapeutic interventions on human hematopoietic lineage-derived cells *in vivo* [14]. This model was used here to validate the effect of ABCB5<sup>+</sup>-derived MSC injection on the M1/M2 wound macrophage phenotype of human origin in NSG iron-overload mice. For this purpose, full-thickness wounds were inflicted on PBMCs humanized NSG mice with subsequent intradermal injection of human allogeneic ABCB5<sup>+</sup>-derived MSCs, donor-matched ABCB5<sup>-</sup> HDFs, or PBS alone into the wound edges. In line with our above findings, accelerated closure of full-thickness wounds upon injection with ABCB5<sup>+</sup>-derived MSCs was observed compared with PBS and ABCB5<sup>-</sup> HDF injection of wounds in PBMC-humanized NSG mice (Fig. 7A). Coimmunostaining of day 5 wounds with human-specific anti-CD68 and either anti-CD206 or anti-TNF $\alpha$  showed a higher number of CD68<sup>+</sup> CD206<sup>+</sup> human M2 macrophages in the wound beds of ABCB5<sup>+</sup>-derived MSC-injected compared with PBS-injected wounds (Fig. 7B). Of note, the number of CD68<sup>+</sup> TNF $\alpha$ <sup>+</sup> proinflammatory macrophages was decreased in ABCB5<sup>+</sup>-derived MSCs compared with PBS-injected wounds (Fig. 7B). Single-cell suspensions derived from day 5 wound tissue were analyzed by multicolor flow cytometry (Supporting Information Fig. S11B) in order to confirm the numbers of human CD68<sup>+</sup> M1 and M2 macrophages at the wound site. The ratio of human M2 to M1 macrophage marker expressing CD68<sup>+</sup> human macrophages was increased in wound tissue treated with ABCB5<sup>+</sup>-derived MSCs compared with PBS for both the ratio of Dectin-1/IL-12p40 and CD206/TNF $\alpha$  expressing cells (Fig. 7C). Even though the humanized model is highly valuable, we cannot fully exclude that the behavior of still existing murine macrophages will be changed by the injection of ABCB5<sup>+</sup> MSCs, and in consequence, may affect human cells. These data indicate that the beneficial anti-inflammatory effect of IL-1RA released from ABCB5<sup>+</sup>-derived MSCs on human wound macrophages was conserved in humanized NSG mice.

## DISCUSSION

We here report that a newly defined dermal cell subpopulation of the skin with MSC characteristics can be successfully isolated from its endogenous niche by a single marker, the P-glycoprotein ABCB5, at high purity and homogeneity. The isolated ABCB5<sup>+</sup> MSC subpopulation reliably maintains the capacity of clonal self-renewal and clonal trilineage differentiation *in vitro*. Our major, previously unreported, finding is that injection of the newly described ABCB5<sup>+</sup> lineage-derived MSCs around wounds—via paracrine IL-1RA release—switch proinflammatory M1 macrophages with unrestrained activation to anti-inflammatory wound repair-promoting M2 macrophages in chronic iron-overload wounds and, in consequence, accelerate impaired wound healing *in vivo* (Graphical Abstract). This constitutes a major preclinical

breakthrough at the forefront of MSC-based therapies in translational medicine that—due to the lack of an appropriate selection marker—so far suffered from therapeutic application of less characterized MSC populations with inconsistent efficacy and potency [27].

The advancement of isolating and expanding MSCs from the skin to high homogeneity depends on the exclusive expression of ABCB5 on MSCs but not on other cells in the skin. Employing a global transcriptomic approach, we here confirmed the existence of dermal ABCB5<sup>+</sup> cells with a MSC characteristic cell surface expression profile [1, 24] and reported coexpression with additional pluripotency and stem cell markers (10–13). We also provide evidence from RNA sequence analysis that ABCB5<sup>+</sup>-enriched MSCs—even when expanded in culture to high passage numbers—keep at least in part their stemness, MSC, and mesenchymal marker expression of endogenous ABCB5<sup>+</sup> cells in the skin. It is, however, unclear whether endogenous ABCB5<sup>+</sup> MSCs and derivatives thereof have a relationship to previously characterized fibroblast lineages [28, 29]. In fact, we found expression of some upper lineage markers of platelet-derived growth factor alpha (PDGF $\alpha$ ) fibroblast lineage tracing mice [28] in ABCB5<sup>+</sup>-derived MSCs, like Prdm1/Blimp-1, a maturation marker for B lymphocytes, and CD26/Dpp4, a dipeptidyl peptidase that cleaves dipeptides from peptides such as growth factors, chemokines, neuropeptides, and vasoactive peptides. We did not find, however, coexpression of ABCB5<sup>+</sup> cells and  $\alpha$ -SMA<sup>+</sup>, a lower scar-promoting fibroblast lineage marker in the skin [28]. These data suggest that the herein used ABCB5<sup>+</sup>-derived MSCs may share some expression features of scar-reducing upper lineage fibroblasts. As to their expression profile, a relationship of ABCB5<sup>+</sup>-derived MSCs to Engrailed-1-derived fibroblast lineages cannot be excluded [29].

Independent of the exact relationship to fibroblast lineages, our major intent was to employ ABCB5 as a single marker for the enrichment of MSCs from skin, to exploit this for MSC-based therapies in difficult-to-treat wounds.

An impressive rescue of impaired wound healing in virtually all studied phases of iron-overload wounds, indeed, depends on enhanced IL-1RA release from injected ABCB5<sup>+</sup>-derived MSCs, which actively shifted prevailing unfavorable M1 macrophages to wound healing-promoting M2 macrophages. This finding is of particular clinical interest given the shared pathogenic role of unrestrained activation of proinflammatory M1 macrophages, causing impaired wound healing in difficult-to-treat chronic wounds in humans [7, 8, 30]. Several lines of evidence support our finding. First, injection of ABCB5<sup>+</sup>-derived MSCs, but not of ABCB5-depleted dermal cells, resulted in enhanced repair of impaired wound healing in iron-overload mice. Within the wound bed of iron-overload mice, M2 macrophages were more abundant after ABCB5<sup>+</sup>-derived MSCs injection in contrast to persisting high numbers of overactivated M1 macrophages as found in iron-overload wounds after injection of either PBS or ABCB5-depleted dermal cell fractions. Second, the occurrence of M2 macrophages in wound beds of ABCB5<sup>+</sup>-derived MSC-injected iron-overload wounds was associated with an increase of anti-inflammatory IL-10, a typical M2 cytokine that suppresses inflammation. At the same time, a decrease of the classical M1 macrophage cytokines TNF $\alpha$ , IL-1, IL-12, and IL-23 only important during early wound healing phases in recruiting and activating microbiocidal M1 macrophages [31] was observed. Third, our previous data showed that under M1 macrophage depleting conditions, iron-overload

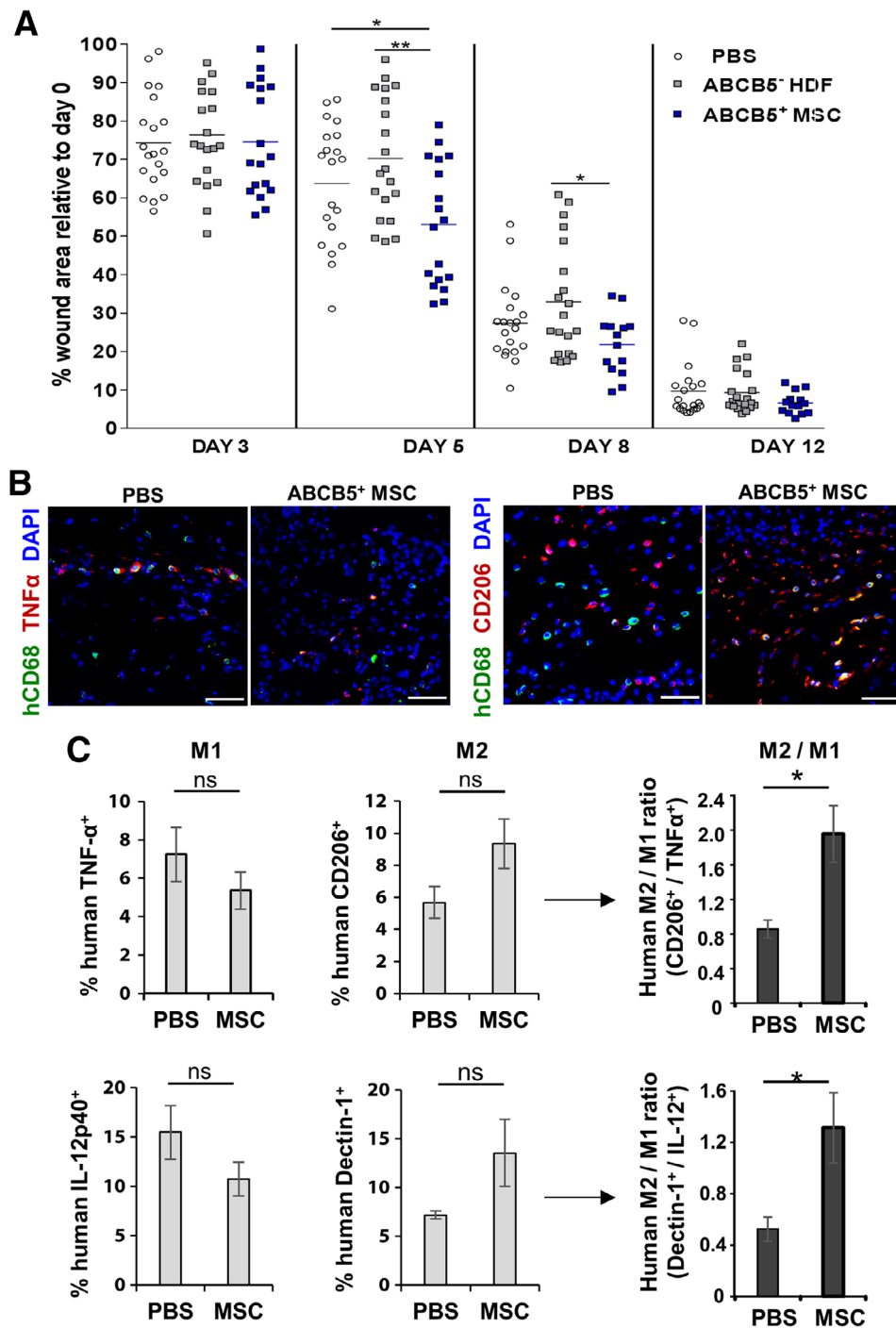


**Figure 7.** ABCB5<sup>+</sup>-derived MSCs stimulate a shift from human M1 macrophages to M2 macrophages in the humanized NOD-*scid* IL2 $\gamma$ <sup>null</sup> (NSG) model. **(A):** Treatment of NSG mouse wounds with ABCB5<sup>+</sup> MSCs led to a significantly reduced wound size compared with control groups at day 5 and day 8. **(B):** Representative microphotographs of day 5 wounds in humanized NSG mice show human CD68<sup>+</sup> macrophages (green) in the wound bed with increased numbers of human inflammatory TNF $\alpha$ <sup>+</sup> (red) macrophages in PBS-treated wounds compared with ABCB5<sup>+</sup>-derived MSC treatment (left panel). Coimmunostaining with M2 marker CD206 (red) displays an MSC-dependent increase in iron-overload wounds (right panel). Nuclei are counterstained with DAPI (blue). Scale bars = 50  $\mu$ m. **(C):** Flow cytometry analysis of human CD68<sup>+</sup>-gated macrophages confirmed the ABCB5<sup>+</sup> MSC-dependent phenotype shift from M1 to M2 with two different costainings. The ratios of both Dectin-1<sup>+</sup>/IL-12p40<sup>+</sup> human macrophages and CD206<sup>+</sup>/TNF $\alpha$ <sup>+</sup> increased after treatment with ABCB5<sup>+</sup> MSCs. ns = not significant; \*,  $p < .05$ ; \*\*,  $p < .01$ ,  $t$  test. Abbreviations: ABCB5, ATP-binding cassette subfamily B member 5; DAPI, 4',6-diamidino-2-phenylindole; HDF, human dermal fibroblasts; IL, interleukin; MSC, mesenchymal stem cells; PBS, phosphate-buffered saline; TNF $\alpha$ , tumor necrosis factor alpha.

wounds depicted a fully restored switch to M2 macrophages with improved wound healing similar to non-iron-overload wounds [7].

As to the question why IL-1RA—apart from IL-1  $\beta$ —can significantly reduce TNF $\alpha$  also, the following scenario is most likely. Both TNF $\alpha$  and to a higher extent IL-1 $\beta$  concentrations are

increased in the iron-overload murine wound model, both cytokines driving activation of inflammatory cells, particularly macrophages. Both IL-1 $\beta$  and TNF $\alpha$  can activate NF $\kappa$ B [32, 33], which itself transactivates target genes such as IL-1 $\beta$ , IL-6, and TNF $\alpha$  among other proinflammatory cytokine and chemokine. In consequence, if IL-1RA neutralizes the high amounts of IL-1 $\beta$ , we expect that the vicious cycle of NF $\kappa$ B activation is significantly reduced with overall less activation and expression of target genes such as IL-1 $\beta$  and TNF $\alpha$ . As IL-1 $\beta$  predominantly enforces its effect via IL-6 induction [32, 34], IL-1RA most likely would impact on overall IL-6 concentrations, and consequently on NF $\kappa$ B activation and downstream target genes. Certainly, we cannot exclude other driver cytokines beyond IL-1 $\beta$  and TNF $\alpha$ . What we though can conclude from our data is that IL-1RA released from ABCB5<sup>+</sup> MSCs does play a causal role in rebalancing the hostile microenvironment of chronic iron-overload wounds.

It is likely that the inflammasome, a multiprotein complex, is responsible for the enhanced release of IL-1 $\beta$  in our iron-overload wound model. In fact, both iron and constituents of bacteria contaminating chronic wounds promote inflammasome overactivation [35, 36]. The role of the inflammasome in acute and chronic tissue damage is complex and far from being fully understood. Transient activation of the inflammasome during physiological wound healing is a prerequisite to coordinate the inflammatory response in defense against microbial invasion and to effectively remove tissue debris [36]. The inflammasome-dependent maturation of IL-1 $\beta$  occurs via cleavage of the propeptide through caspase 1 and is necessary to recruit and activate neutrophils and macrophages to the site of injury. Inhibition of this inflammasome-dependent maturation step of IL-1 $\beta$  in mice deficient for caspase 1 revealed delayed wound healing [37]. Unrestrained activation of IL-1 $\beta$  in mice deficient of the IL-1RA resulted in a fibrotic response of lung tissue in a model of chlamydia pneumonia infection [38]. Similar to our data, persistent inflammasome-dependent activation of IL-1 $\beta$  in diabetic mice also correlates with delayed wound healing of skin wounds [39], which can be almost completely restored to normal healing by suppression of the inflammasome [40]. Our findings in conjunction with the above reports show that balanced inflammasome activation is crucial for coordinated tissue repair, and if this balance is disrupted, wound healing will be impaired.

Descriptive evidence that MSCs dampen single aspects of macrophage activation in vitro [16, 17, 41–43] and even in acute wound models has been reported [16, 17, 43, 44]. However, a thorough characterization of the switch from M1 to M2 macrophages or the responsible paracrine mechanism is lacking. Therefore, the present approach highlights the usefulness of a more complete assessment of the paracrine effects of ABCB5<sup>+</sup>-derived MSCs on healing of chronic wounds and helped to identify IL-1RA as the key effector molecule responsible for a rigorous switch from proinflammatory, detrimental M1 macrophages to anti-inflammatory M2 macrophages.

Our data on the paracrine effect of IL-1RA released from ABCB5<sup>+</sup>-derived MSCs are in line with previous findings [45]. In this regard, IL-1RA knockout mice displayed delayed wound healing of acute wounds [45]. Furthermore, improved healing was reported in mice with a targeted deletion of the IL-1 receptor (IL-1R) or after treatment with recombinant IL-1RA of acute wounds of wild-type mice [46] and of diabetic mice [8]. IL-1RA secretion from less well-characterized MSCs has been described to be beneficial in a variety

of pathological conditions in preclinical studies [47]. We here distinctly advance our understanding that the shift from the unrestrained proinflammatory M1 to the anti-inflammatory M2 macrophages is due to the beneficial IL-1RA effects reliably controlling macrophage-dominated tissue inflammation.

In line with our concept and data, there is clear evidence from the literature [48] that human IL-1RA can efficiently bind to murine cells with a high affinity and thereby inhibit murine IL-1 $\beta$  binding and signaling. In this regard, human IL-1RA has earlier been shown to bind to the type I IL-1 receptor on murine cells with an affinity of 150 pM, equal to the binding of human IL-1 $\alpha$  and IL-1 $\beta$ .

Our findings cannot exclude that, in addition to IL1RA, other mechanisms may contribute to counteract tissue damage because of the unrestrained M1 macrophage activation. In fact, several investigators including ourselves have earlier shown that MSCs dampen inflammation and, in consequence, reduce scar formation in tissue repair via the release of TSG-6 [17, 49]. By contrast to accelerated healing of full-thickness wounds following TSG-6 release from MSCs injected at the wound site [17], although TSG-6 was expressed at the wound site of iron-overload wounds, TSG-6 apparently does not play a major role in accelerating healing of iron-overload wounds. In fact, injection of recombinant TSG-6 at concentrations that enhance acute wound healing does not enhance healing of iron-overload wounds. Differences in the microenvironment will be sensed by injected MSCs, which, in consequence, may raise different adaptive responses in terms of the anti-inflammatory factors released.

Apart from IL-1RA, other factors may contribute to the accelerated healing. In this regard, MSCs have been reported to suppress oxidative damage during sepsis via PGE2-dependent reprogramming of macrophages to increase the release of anti-inflammatory IL-10 [50]. In addition, by enhanced IL-6 and TGF- $\beta$  release, MSCs inhibit neutrophil recruitment by cytokine-activated endothelial cells [51].

A minor limitation of the murine wound model used is the modest delay in wound closure compared with nonhealing CVU in patients. Nevertheless, this model mimics the iron-induced unrestrained activation of wound M1 macrophages with prolonged inflammation and tissue breakdown and, hence, represents a well-suited model to study the effect of treatment strategies on these specific pathophysiological traits [7].

## CONCLUSION

In aggregate, our findings have substantial clinical impact for the planned implementation into clinical routine. Here, we first uncovered the adaptive release of a key factor efficiently dampening unrestrained M1 macrophage-dominated inflammation underlying dysregulated tissue repair in iron-overload chronic wounds. Second, the employment of a single marker strategy allows the enrichment of an easily accessible homogeneous ABCB5<sup>+</sup>-derived MSC population from human skin with GMP grade quality, ready to use for transition into clinics. Third, we developed an in vitro assay predictive for the successful action of the used MSC preparations in a chronic murine wound model. ABCB5<sup>+</sup>-derived MSC preparations from different donors, alone or pooled, successfully suppressed the release of M1 macrophage cytokines, and this suppressive effect correlated well with

the improvement of healing when the corresponding ABCB5<sup>+</sup>-derived MSCs were injected into iron-overload wounds.

Thus, the above data reveal enhanced efficacy and potency of the newly described dermal ABCB5<sup>+</sup>-derived MSCs, which hold substantial promise for the successful clinical therapy of nonhealing wounds. In fact, clinical phase IIa studies have recently been initiated (EudraCT number: 2015-000399-81, 2017-000233-31, 000234-57) with promising results of the first studied patients.

#### ACKNOWLEDGMENTS

S.V.B. is currently affiliated with the Bredent medical GmbH & Co.KG, Senden, Germany; B.M.-S. is currently affiliated with the Department of Dermatology, University Hospital Zürich, Zürich, Switzerland. We thank Dr. L.A. Schneider, Dr. M. Mühlberger, and Dr. K. Hefele (University Clinic Ulm) for providing human skin samples. This study was supported in part by research grants from the Baden-Württemberg Stiftung (P-BWS-ASII/15), the European Commission (CASCADE HEALTH-FP7-223236), and the German Research Foundation (SFB1149) to K.S.-K. as well as the Baustein Program from the Medical Faculty, University of Ulm (LSBN.0100) to D.J. and S.V.B. This work was also in part funded by RHEACELL GmbH & Co. KG and also supported in part by NIH grants R01EY025794 and R24EY028767 (to M.H.F. and N.Y.F.) and the Department of Veterans Affairs VA Merit Review Awards VA BLR&D 1I01BX000516 and VA RR&D 1I01RX000989 (to N.Y.F.).

#### AUTHOR CONTRIBUTIONS

S.V.B.: collection and/or assembly of data, data analysis and interpretation, conception/design, set up experiments, administrative support, supervision, manuscript writing; J.C.de.V., P. Meyer: collection and/or assembly of data, data analysis and interpretation, conception/design, set up experiments; B.M.-S.: collection and/or assembly of data, data analysis and interpretation, conception/design, set up experiments; D.J.: collection and/or assembly of data, data analysis and interpretation, conception/design, set up experiments, administrative support, supervision; A.S., M.W.: conception/design, set up experiments, administrative support, supervision; F.F.F., J.M., N.J.S.: technical support; A.H., S.S.: collection and/or assembly of data, data analysis and interpretation, technical support; P.K.: isolated and provided ABCB5<sup>+</sup> and ABCB5<sup>-</sup> cell fractions; A.M.S.: collection and/or assembly of data, data analysis

and interpretation, conception/design, administrative support, technical support; L.D.: conception/design, set up experiments, administrative support, technical support; A.I.: conception/design, set up experiments, administrative support, technical support; M.A.K.: collection and/or assembly of data, data analysis and interpretation, isolated and provided ABCB5<sup>+</sup> and ABCB5<sup>-</sup> cell fractions; C.G.: isolated and provided ABCB5<sup>+</sup> and ABCB5<sup>-</sup> cell fractions, isolated and provided ABCB5<sup>+</sup> and ABCB5<sup>-</sup> cell fractions; K.S., P. Maity: collection and/or assembly of data, data analysis and interpretation; N.Y.F.: conception/design, set up experiments, provision of anti-ABCB5 monoclonal antibody; M.H.F.: conception/design, set up experiments, provision of anti-ABCB5 monoclonal antibody, manuscript writing; K.S.-K.: conception/design, set up experiments, administrative support, supervision, manuscript writing, final approval of manuscript.

#### DISCLOSURE OF POTENTIAL CONFLICTS OF INTEREST

M.H.F. serves as a scientific advisor to Ticeba GmbH and Rheacell GmbH & Co. KG, has participated in corporate sponsored research collaborations with Rheacell GmbH & Co. KG, also holds a U.S. patent on ABCB5<sup>+</sup> MSCs with the number US 2013/0315880 A1 assigned to Brigham and Women's Hospital and/or Boston Children's Hospital, Boston, MA, and licensed to Ticeba GmbH (Heidelberg, Germany) and Rheacell GmbH & Co. KG (Heidelberg, Germany), and received corporate sponsored research collaborations with Rheacell GmbH & Co. KG. C.G. declares leadership position and shareholder in Ticeba GmbH (Heidelberg, Germany) and Rheacell GmbH & Co. KG (Heidelberg, Germany). M.H.F. and N.Y.F. are inventors of issued or pending ABCB5-related U.S. patents assigned to Boston Children's Hospital and/or Brigham and Women's Hospital, Boston, MA, and licensed to Ticeba GmbH (Heidelberg, Germany) and Rheacell GmbH & Co. KG (Heidelberg, Germany). M.A.K. declared research funding from Ticeba GmbH (Heidelberg, Germany) and Rheacell GmbH & Co. KG (Heidelberg, Germany). The other authors indicated no potential conflicts of interest.

#### DATA AVAILABILITY

The RNASeq data were uploaded in GEO with accession number GEO GSE125829. The 2,906 base pair ABCB5 cDNA sequence reported in 2003 [11] can be found at NCBI GenBank under accession number AY234788.

#### REFERENCES

- 1 Lv FJ, Tuan RS, Cheung KM et al. Concise review: The surface markers and identity of human mesenchymal stem cells. *STEM CELLS* 2014;32:1408–1419.
- 2 Vishnubalaji R, Al-Nbaheen M, Kadalmani B et al. Skin-derived multipotent stromal cells—An archival for mesenchymal stem cells. *Cell Tissue Res* 2012;350:1–12.
- 3 Fukada S, Ma Y, Uezumi A. Adult stem cell and mesenchymal progenitor theories of aging. *Front Cell Dev Biol* 2014;2:10.
- 4 Sen CK, Gordillo GM, Roy S et al. Human skin wounds: A major and snowballing threat to public health and the economy. *Wound Repair Regen* 2009;17:763–771.
- 5 Schatton T, Yang J, Kleffel S et al. ABCB5 identifies immunoregulatory dermal cells. *Cell Rep* 2015;12:1564–1574.
- 6 Ksander BR, Kolovou PE, Wilson BJ et al. ABCB5 is a limbal stem cell gene required for corneal development and repair. *Nature* 2014;511:353–357.
- 7 Sindrilaru A, Peters T, Wieschalka S et al. An unrestrained proinflammatory M1 macrophage population induced by iron impairs wound healing in humans and mice. *J Clin Invest* 2011;121:985–997.
- 8 Mirza RE, Fang MM, Ennis WJ et al. Blocking interleukin-1beta induces a healing-associated wound macrophage phenotype and improves healing in type 2 diabetes. *Diabetes* 2013;62:2579–2587.
- 9 Sindrilaru A, Scharffetter-Kochanek K. Disclosure of the culprits: Macrophages-versatile regulators of wound healing. *Adv Wound Care* 2013;2:357–368.
- 10 Peters T, Sindrilaru A, Hinz B et al. Wound-healing defect of CD18(−/−) mice due to a decrease in TGF-beta1 and myofibroblast differentiation. *EMBO J* 2005;24:3400–3410.
- 11 Frank NY, Pendse SS, Lapchak PH et al. Regulation of progenitor cell fusion by ABCB5 P-glycoprotein, a novel human ATP-binding cassette transporter. *J Biol Chem* 2003;278:47156–47165.

- 12 Singh K, Krug L, Basu A et al. Alpha-ketoglutarate curbs differentiation and induces cell death in mesenchymal stromal precursors with mitochondrial dysfunction. *STEM CELLS* 2017; 35:1704–1718.
- 13 Gregory CA, Gunn WG, Peister A et al. An Alizarin red-based assay of mineralization by adherent cells in culture: Comparison with cetylpyridinium chloride extraction. *Anal Biochem* 2004;329:77–84.
- 14 Pearson T, Greiner DL, Shultz LD. Creation of "humanized" mice to study human immunity. *Curr Protoc Immunol*. 2008; Chapter 15: Unit 15.21.
- 15 Singh K, Maity P, Krug L et al. Superoxide anion radicals induce IGF-1 resistance through concomitant activation of PTP1B and PTEN. *EMBO Mol Med* 2015;7:59–77.
- 16 Jiang D, Qi Y, Walker NG et al. The effect of adipose tissue derived MSCs delivered by a chemically defined carrier on full-thickness cutaneous wound healing. *Biomaterials* 2013; 34:2501–2515.
- 17 Qi Y, Jiang D, Sindrilaru A et al. TSG-6 released from intradermally injected mesenchymal stem cells accelerates wound healing and reduces tissue fibrosis in murine full-thickness skin wounds. *J Invest Dermatol* 2014;134: 526–537.
- 18 Singh K, Camera E, Krug L et al. JunB defines functional and structural integrity of the epidermo-pilosebaceous unit in the skin. *Nat Commun* 2018;9:3425.
- 19 Henderson JK, Draper JS, Baillie HS et al. Preimplantation human embryos and embryonic stem cells show comparable expression of stage-specific embryonic antigens. *STEM CELLS* 2002;20:329–337.
- 20 Bartsch G, Yoo JJ, De Coppi P et al. Propagation, expansion, and multilineage differentiation of human somatic stem cells from dermal progenitors. *Stem Cells Dev* 2005;14: 337–348.
- 21 Battula VL, Bareiss PM, Tremel S et al. Human placenta and bone marrow derived MSC cultured in serum-free, b-FGF-containing medium express cell surface frizzled-9 and SSEA-4 and give rise to multilineage differentiation. *Differentiation* 2007;75:279–291.
- 22 Gang EJ, Bosnakovski D, Figueiredo CA et al. SSEA-4 identifies mesenchymal stem cells from bone marrow. *Blood* 2007;109:1743–1751.
- 23 Ozerdem U, Grako KA, Dahlin-Huppe K et al. NG2 proteoglycan is expressed exclusively by mural cells during vascular morphogenesis. *Dev Dyn* 2001;222:218–227.
- 24 Dominici M, Le Blanc K, Mueller I et al. Minimal criteria for defining multipotent mesenchymal stromal cells. The International Society for Cellular Therapy position statement. *Cytotherapy* 2006;8:315–317.
- 25 Muraglia A, Cancedda R, Quarto R. Clonal mesenchymal progenitors from human bone marrow differentiate in vitro according to a hierarchical model. *J Cell Sci* 2000;113:1161–1166.
- 26 Vaculik C, Schuster C, Bauer W et al. Human dermis harbors distinct mesenchymal stromal cell subsets. *J Invest Dermatol* 2012; 132:563–574.
- 27 Phinney DG. Functional heterogeneity of mesenchymal stem cells: Implications for cell therapy. *J Cell Biochem* 2012;113:2806–2812.
- 28 Driskell RR, Lichtenberger BM, Hoste E et al. Distinct fibroblast lineages determine dermal architecture in skin development and repair. *Nature* 2013;504:277–281.
- 29 Rinkevich Y, Walmsley GG, Hu MS et al. Identification and isolation of a dermal lineage with intrinsic fibrogenic potential. *Science* 2015;348:aaa2151.
- 30 Tsourdi E, Barthel A, Rietzsch H et al. Current aspects in the pathophysiology and treatment of chronic wounds in diabetes mellitus. *Biomed Res Int* 2013;2013:1–6.
- 31 Mosser DM, Edwards JP. Exploring the full spectrum of macrophage activation. *Nat Rev Immunol* 2008;8:958–969.
- 32 Wietek C, O'Neill LA. Diversity and regulation in the NF-kappaB system. *Trends Biochem Sci* 2007;32:311–319.
- 33 Ozes ON, Mayo LD, Gustin JA et al. NF-kappaB activation by tumour necrosis factor requires the Akt serine-threonine kinase. *Nature* 1999;401:82–85.
- 34 Cahill CM, Rogers JT. Interleukin (IL) 1beta induction of IL-6 is mediated by a novel phosphatidylinositol 3-kinase-dependent AKT/IkappaB kinase alpha pathway targeting activator protein-1. *J Biol Chem* 2008;283:25900–25912.
- 35 Nakamura K, Kawakami T, Yamamoto N et al. Activation of the NLRP3 inflammasome by cellular labile iron. *Exp Hematol* 2016;44: 116–124.
- 36 Artlett CM. Inflammasomes in wound healing and fibrosis. *J Pathol* 2013;229:157–167.
- 37 Lee DJ, Du F, Chen SW et al. Regulation and function of the Caspase-1 in an inflammatory microenvironment. *J Invest Dermatol* 2015;135:2012–2020.
- 38 He X, Mekasha S, Mavrogiorgos N et al. Inflammation and fibrosis during Chlamydia pneumoniae infection is regulated by IL-1 and the NLRP3/ASC inflammasome. *J Immunol* 2010; 184:5743–5754.
- 39 Mirza RE, Fang MM, Weinheimer-Haus EM et al. Sustained inflammasome activity in macrophages impairs wound healing in type 2 diabetic humans and mice. *Diabetes* 2014;63:1103–1114.
- 40 Bitto A, Altavilla D, Pizzino G et al. Inhibition of inflammasome activation improves the impaired pattern of healing in genetically diabetic mice. *Br J Pharmacol* 2014;171:2300–2307.
- 41 Kim J, Hematti P. Mesenchymal stem cells convert human macrophages to a novel type of alternatively activated macrophages. *Blood* 2009;114:1403–1403.
- 42 Maggini J, Mirkin G, Bognanni I et al. Mouse bone marrow-derived mesenchymal stromal cells turn activated macrophages into a regulatory-like profile. *Plos One* 2010;5: e9252.
- 43 Zhang QZ, Su WR, Shi SH et al. Human gingiva-derived mesenchymal stem cells elicit polarization of m2 macrophages and enhance cutaneous wound healing. *STEM CELLS* 2010;28: 1856–1868.
- 44 Nakajima H, Uchida K, Guerrero AR et al. Transplantation of mesenchymal stem cells promotes an alternative pathway of macrophage activation and functional recovery after spinal cord injury. *J Neurotrauma* 2012;29:1614–1625.
- 45 Ishida Y, Kondo T, Kimura A et al. Absence of IL-1 receptor antagonist impaired wound healing along with aberrant NF-kappaB activation and a reciprocal suppression of TGF-beta signal pathway. *J Immunol* 2006;176: 5598–5606.
- 46 Thomay AA, Daley JM, Sabo E et al. Disruption of interleukin-1 signaling improves the quality of wound healing. *Am J Pathol* 2009;174:2129–2136.
- 47 Meier RP, Mahou R, Morel P et al. Micro-encapsulated human mesenchymal stem cells decrease liver fibrosis in mice. *J Hepatol* 2015; 62:634–641.
- 48 Dripps DJ, Brandhuber BJ, Thompson RC et al. Interleukin-1 (IL-1) receptor antagonist binds to the 80-kDa IL-1 receptor but does not initiate IL-1 signal transduction. *J Biol Chem* 1991;266:10331–10336.
- 49 Liu S, Jiang L, Li H et al. Mesenchymal stem cells prevent hypertrophic scar formation via inflammatory regulation when undergoing apoptosis. *J Invest Dermatol* 2014;134: 2648–2657.
- 50 Nemeth K, Leelahavanichkul A, Yuen PS et al. Bone marrow stromal cells attenuate sepsis via prostaglandin E(2)-dependent reprogramming of host macrophages to increase their interleukin-10 production. *Nat Med* 2009; 15:42–49.
- 51 Luu NT, McGettrick HM, Buckley CD et al. Crosstalk between mesenchymal stem cells and endothelial cells leads to downregulation of cytokine-induced leukocyte recruitment. *STEM CELLS* 2013;31:2690–2702.



See [www.StemCells.com](http://www.StemCells.com) for supporting information available online.